

Dark Radiation with Baryon Acoustic Oscillations from DESI 0 and the H_0 tension 0

Itamar J. Allali,^{1,*} Alessio Notari,^{2,3,†} and Fabrizio Rompineve^{4,5,‡}

¹*Department of Physics, Brown University, Providence, RI 02912, USA*

²*Departament de Física Quàntica i Astrofísica & Institut de Ciències del Cosmos (ICCUB),*

Universitat de Barcelona, Martí i Franquès 1, 08028 Barcelona, Spain.

³*Galileo Galilei Institute for theoretical physics,*

Centro Nazionale INFN di Studi Avanzati Largo Enrico Fermi 2, I-50125, Firenze, Italy

⁴*Departament de Física, Universitat Autònoma de Barcelona, 08193 Bellaterra, Barcelona, Spain*

⁵*Institut de Física d'Altes Energies (IFAE) and The Barcelona Institute of Science and Technology (BIST),*

Campus UAB, 08193 Bellaterra (Barcelona), Spain

We investigate the presence of extra relativistic degrees of freedom in the early Universe, contributing to the effective number of neutrinos N_{eff} , as $\Delta N_{\text{eff}} \equiv N_{\text{eff}} - 3.044 \geq 0$, in light of the recent measurements of Baryon Acoustic Oscillations (BAO) by the DESI collaboration. We analyze one-parameter extensions of the Λ CDM model where dark radiation (DR) is free streaming or behaves as a perfect fluid, due to self-interactions. We report a significant relaxation of upper bounds on ΔN_{eff} , with respect to previous BAO data from SDSS+6dFGS, when additionally employing *Planck* data (and supernovae data from *Pantheon+*), setting $\Delta N_{\text{eff}} < 0.39$ (95% C.L.) for free streaming DR, and a very mild preference for fluid DR, $\Delta N_{\text{eff}} = 0.221^{+0.088}_{-0.18}$ (≤ 0.46 , 95% C.L.). Applying constraints from primordial element abundances leads to slightly tighter constraints on ΔN_{eff} , but they are avoided if DR is produced after Big Bang Nucleosynthesis (BBN). For fluid DR we estimate the tension with the SH₀ES determination of H_0 to be less than 3σ and as low as 2σ , and for free-streaming DR the tension is below 3σ if production occurs after BBN. This lesser degree of tension motivates a combination with SH₀ES in these cases, resulting in a $4.4\sigma - 5\sigma$ evidence for dark radiation with $\Delta N_{\text{eff}} \simeq 0.6$ and large improvements in χ^2 over Λ CDM, $-18 \lesssim \Delta\chi^2 \lesssim -25$.

I. Introduction 3

Modern cosmological datasets are among the most powerful probes of physics beyond the Standard Model (SM), even when this has negligible interactions with SM particles. This is particularly true if new physics is in the form of light degrees of freedom that remain ultra-relativistic throughout the cosmological evolution, until after the epoch of recombination. Their additional contribution to the energy density impacts the background expansion and density perturbations in the early Universe, when the Cosmic Microwave Background (CMB) is produced (see [1, 2] and [3]). Finding evidence for such *dark radiation* (DR), or alternatively constraining its presence to unprecedented levels, is one of the main targets of active and future cosmological surveys [4–9], and has a potentially groundbreaking impact on fundamental physics. 4

The aim of this *Letter* is to assess the status of DR in light of the new measurements of Baryon Acoustic Oscillations (BAO) from galaxies and quasars [10] at redshifts $0.3 \lesssim z \lesssim 1.5$ and from the Lyman- α forest [11] by the Dark Energy Spectroscopic Instrument [12] (DESI). 5

BAO data from previous galactic surveys [13–15] have so far provided the most stringent constraints on

DR, when combined with CMB measurements from the *Planck* satellite [16] (Big Bang Nucleosynthesis and measurements of primordial element abundances provide an alternative probe, though one with possibly larger uncertainties, see e.g. the discussion in [17], and [18] for a recent update). In terms of the customary parameterization of the abundance of DR, given by the *effective number of neutrino species*, i.e. $\Delta N_{\text{eff}} \equiv \rho_{\text{DR}}/\rho_\nu$, where ρ_ν is the energy density of a single neutrino species, the DESI collaboration has recently reported $\Delta N_{\text{eff}} \leq 0.40$ (95% C.L.) [12] for free streaming species. Interestingly, this is a significant relaxation of the previous CMB+BAO bound $\Delta N_{\text{eff}} \leq 0.28$ [16] (95% C.L., with fixed sum of neutrino masses $\sum m_\nu = 0.06$ eV). Both these results were obtained allowing for $\Delta N_{\text{eff}} < 0$ in the prior. 6

While the ΔN_{eff} parameterization effectively captures a vast landscape of particle physics scenarios, the specific microphysical origin of DR can lead to different imprints on cosmological observables. Perhaps the simplest model dependence arises between the case where DR is free streaming (some well motivated examples are: the QCD axion with a small mass [19–27] and relic gravitational waves, see also [28] for other candidates), and the possibility that it behaves as a perfect fluid with equation of state parameter $w = 1/3$ (see e.g. the discussion in [3]). This latter case applies to a self-interacting gas of relativistic particles (as can arise e.g. in dark sector models with gauge interactions [29–32]), see [33–38] for investigations with previous data, and to scalar fields that start oscillating in quartic potentials well

* itamar.allali@brown.edu 1

† notari@fqa.ub.edu 1

‡ frompineve@ifae.es 1

before recombination. A different simple scenario that is captured by ΔN_{eff} is one where the abundance of neutrinos differs from the prediction of the SM, as can be the case if neutrinos or photons are slightly reheated by a dark sector after their decoupling (i.e. at temperatures below MeV).⁷

The first aim of this work is thus to provide the state-of-the-art constraints on such simplest DR scenarios, also accounting for data from additional cosmological observations, such as measurements of the Hubble diagram from supernovae [39] and of primordial element abundances. These can then be used by particle physicists to determine bounds on microphysical models.

Our findings then lead to the second aim of our work. We indeed interestingly find that the new BAO data allow for larger abundances of DR in all cases of study, which motivates a reassessment of whether such simple one parameter extensions of the Λ CDM model can reconcile the value of the Hubble expansion parameter H_0 inferred from fitting to cosmological datasets, with the larger value measured from supernovae [40] (see also [41–43] for other measurements).⁹

II. Models and datasets¹²

We limit our study to the following three simple realizations of DR, all effectively captured by a single parameter $\Delta N_{\text{eff}} \equiv N_{\text{eff}} - 3.044$, where the latter contribution comes from SM neutrinos:¹³

- **Free-streaming:** these species, assumed to be massless, have large anisotropic stress [1] that produces a phase shift in CMB anisotropies.¹⁴
- **Fluid:** there is no anisotropic stress, thus the perturbation equations are the Euler and continuity equations of perfect adiabatic fluid with $w = c_s^2 = 1/3$ [44]. The extra species is still assumed to be massless.¹⁴
- **Neutrinos:** we allow for the SM neutrino temperature to differ from that predicted by the SM (both larger or smaller), while keeping the free-streaming nature of neutrinos.¹⁴

The first two models have exactly the same background evolution, and differ only at the level of perturbations. While strictly speaking the species are described as massless, the ΔN_{eff} parametrization effectively captures any scenario where the mass is somewhat below 0.05 eV.

The third model differs at both levels, since SM neutrinos have a non-negligible mass around and after recombination. Throughout our work, we take neutrinos to be degenerate in mass and temperature and impose the prior¹⁶ $m_\nu > 0.06$ eV from neutrino oscillations. We therefore always add¹⁶ m_ν as an additional free cosmological parameter to the Λ CDM model.¹ For the

first two models above, the neutrino sector is not altered with respect to the SM prediction, and thus a prior $\Delta N_{\text{eff}} \geq 0$ is imposed.²¹⁶

We perform Bayesian searches using CLASS [45, 46] to solve for the cosmological evolution and MontePython [47, 48] to collect Markov Chain Monte Carlo (MCMC) samples. We obtain posteriors and figures using GetDist [49]. We consider the following datasets in our searches:¹⁷

• **P18:** Planck 2018 high- ℓ and low- ℓ TT, TE, EE and lensing data [17];¹⁸

• **+DESI:** BAO measurements from DESI 2024 [12];¹⁹

• **+SDSS+6dFGS:** BAO measurements from 6dFGS at $z = 0.106$ [13], SDSS MGS at $z = 0.15$ [14] (BAO smallz), and CMASS and LOWZ galaxy samples of BOSS DR12 at $z = 0.38, 0.51$, and 0.61 [50]. We use this only in alternative to DESI BAO data;²⁰

• **+Pantheon Plus.** The Pantheon+ supernovae compilation [39]. We use the Pantheon Plus likelihood in MontePython;²³

• **+Y_{He}, D/H:** measurements of the abundance of primordial elements from [51] for Helium and [52] for Deuterium. The theoretical prediction for Y_{He} at BBN is determined using [53] and PArthENoPE v 1.10, as implemented in the likelihood bbn in MontePython;²²

• **+H₀:** the latest measurement of the intrinsic SNIa magnitude $M_b = -19.253 \pm 0.027$ from the SH0ES collaboration [40]. We add this only in combination with Pantheon+ data, as consistently implemented in the Pantheon_Plus_SH0ES likelihood in MontePython;²¹

For the purposes of setting constraints, we will consider the combination **P18+DESI+Pantheon_Plus** to be our baseline dataset (comparing also to the case with **+DESI** exchanged for **+SDSS+6dFGS**). Weaker bounds from **P18+DESI** alone are reported in App. B1. The **+Y_{He}, D/H** dataset is used to generate constraints when appropriate. And finally, the **+H₀** dataset is used when interpreting the H_0 tension as a moderate statistical fluctuation.²⁴

¹ This has however little impact on our results, as already discussed in [17, 30]

² This differs from the choice of the DESI collaboration, the prior choice of which allows neutrinos to be colder than as predicted by the SM.¹⁶

Parameter	P18+DESI+Pantheon_Plus			+Y _{He} , D/H	
	Free-streaming	Fluid	Neutrinos	Free-streaming	Fluid
ΔN_{eff}	< 0.386	0.221 ^{+0.083} _{-0.18} 100	0.06 ^{+0.17} _{-0.19} 10	< 0.295	< 0.365 2
H_0 [km/s/Mpc]	68.79 ^{+0.66} _{-0.89} 90	69.35 ^{+0.51} _{-1.1} 90	68.0 ^{+1.0} _{-1.2} 1	68.62 ^{+0.53} _{-0.76} 10	68.97 ^{+0.65} _{-0.93} 62
H_0 GT	3.53σ	2.81σ	3.43σ	3.79σ	3.31σ 10
H_0 IT	3.06σ	2.52σ	3.24σ	3.4σ	2.93σ 10

TABLE I: Marginalized posteriors for ΔN_{eff} and H_0 . Two models for dark radiation are considered: free-streaming and perfect fluid. We report results with our baseline dataset, and additionally adding measurements of primordial abundances. We report upper bounds on ΔN_{eff} at 95% C.L. for all models and datasets, except for the fluid model fitted to the baseline dataset, where a 1σ preference for dark radiation is found (the 95% C.L. upper bound is $\Delta N_{\text{eff}} < 0.461$). The corresponding tension with the SH₀ES measurement is also reported. Posteriors for all parameters are reported in Appendices B 2 and B 5 for the baseline and +Y_{He}, D/H datasets, respectively. 11

III. New constraints on dark radiation 25

Let us first focus on the impact of the new BAO data from DESI on DR models. We fit the models of free-streaming and fluid DR to the baseline dataset, and compare this to the case where previous BAO data are used instead of DESI BAO. Posteriors for ΔN_{eff} and H_0 are shown in Fig. 1. One can immediately appreciate the qualitative difference in the results: for both free-streaming and fluid DR, the 1 and 2σ regions of the posteriors extend to larger values of ΔN_{eff} , indicating that the DESI BAO data allow for larger abundances of DR. The new 95% C.L. constraints are reported in Table I, and show a significant relaxation of up to 20% for free-streaming DR with respect to using +SDSS+6dFGS, see Appendix B 7 (our 95% C.L. upper bound on ΔN_{eff} agrees with [12], despite our different prior choice; the central value is however shifted to larger values than in [12], as expected). The situation is even more interesting for the fluid DR scenario: the 1d marginalized posterior for ΔN_{eff} is shifted to larger values, and a non vanishing abundance $\Delta N_{\text{eff}} \approx 0.2$ is now (very mildly) preferred at 1σ . We report further posteriors in Table I. In particular, for the neutrino model we find that deviations of up to 6% from the SM abundance are allowed. In all our runs we find similar upper bounds $m_\nu \leq 0.12 \sim 0.13$ eV. Full posteriors for all models and cosmological parameters are reported in Appendix B 26

The DR abundance allowed by the new BAO data is potentially independently constrained by observations of light element abundances. We therefore examine the impact of these measurements using the +Y_{He}, D/H dataset. We report the resulting upper bounds on ΔN_{eff} in Table I. One can see that the mild preference for $\Delta N_{\text{eff}} > 0$ in the fluid case is erased by the +Y_{He}, D/H data. Constraints on ΔN_{eff} become significantly tighter for the free-streaming case as well.³

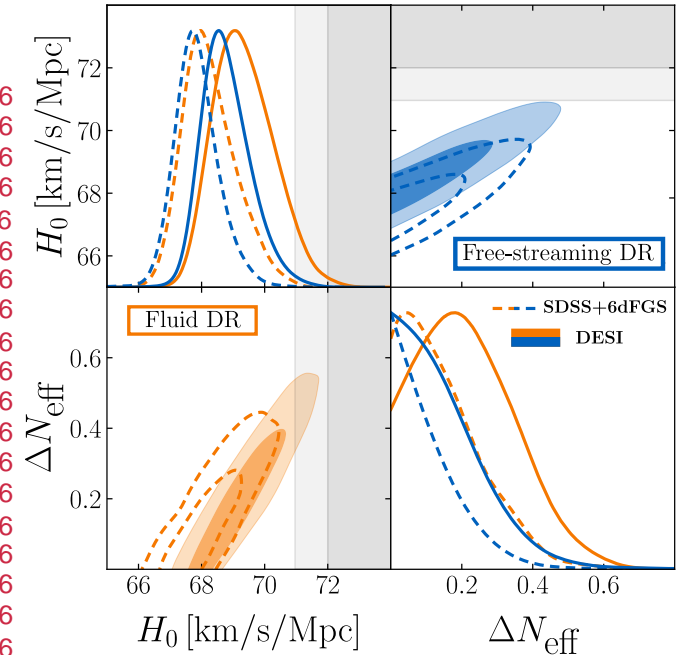


FIG. 1: 1- and 2-d posterior distributions for H_0 and ΔN_{eff} in dark radiation models, obtained using our baseline dataset. We compare our results with the new DESI BAO data (solid curves/shaded contours) with those obtained with previous BAO data (dashed curves/contours). The 68% and 95% confidence intervals from the measurement of H_0 by SH₀ES are shown in the gray and lighter gray shaded regions. 28

Note that measurements of primordial elements exist, which disagree with those that we have used (see e.g. [16, 54] for a summary). For instance, using [55] rather than [51] would lead to significant evidence for ΔN_{eff} (as noted similarly for free streaming DR in [16, 56]). 27

We now move to H_0 , and highlight two interesting effects of the new BAO data: first, larger values are preferred, even in the absence of dark radiation. Second, the alleviated constraints on ΔN_{eff} allow for even larger values of H_0 , given the strong degeneracy between these two parameters. For comparison, the SH₀ES 31

³ We do not highlight here the results for neutrinos (see however Appendix B 5), since modifying the neutrino abundance can most plausibly be achieved after BBN. 27

Parameter	P18+DESI+Pantheon_Plus		+H ₀ 94	
	Free-streaming DR	Fluid DR	Free-streaming DR	Fluid DR 62
ΔN_{eff}	< 0.435	0.26 (0.34) ^{+0.11} _{-0.21} 90	0.63 (0.56) \pm 0.14	0.65 (0.73) \pm 0.13 29
$H_0 [\text{km/s/Mpc}]$	68.94 (68.41) ^{+0.63} _{-0.99} 90	69.56 (69.82) ^{+0.83} _{-1.2} 94	71.82 (71.65) ^{+0.78} _{-0.77} 29	72.26 (73.0) ^{+0.77} _{-0.78} 29
H_0 GT	3.37σ	2.59σ	0.94σ	0.6σ 29
H_0 IT	2.84σ	2.28σ	0.94σ	0.6σ 29
$\Delta\chi^2$	~ 0	-0.4	-20.5	-24.7 29
ΔAIC	+2.0	+1.6	-18.5	-22.7 29

TABLE II: Marginalized posteriors for ΔN_{eff} and H_0 for scenarios where dark radiation is produced after BBN. Two models are considered: free-streaming and fluid DR. We report results with our baseline dataset, and additionally adding the determination of H_0 from SH₀ES. The corresponding tension with the SH₀ES measurement is also reported, as well as two measures of goodness-of-fit compared to the Λ CDM model. Posteriors for all parameters are reported in Appendices B 8 and B 9. 30

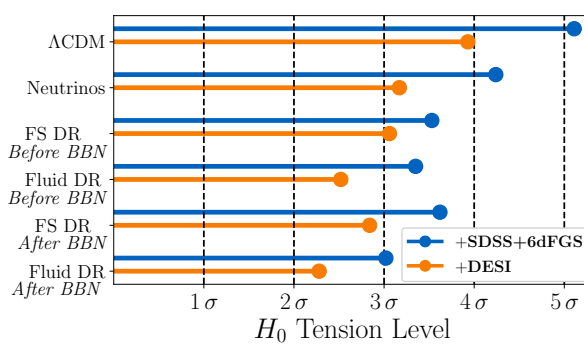


FIG. 2: Measure of the tension (IT, see Appendix A) in the determinations of H_0 from the P18+DESI+Pantheon_Plus dataset with respect to the SH₀ES measurement, for models considered in this work. Results with previous BAO data are shown for comparison. FS refers to “free-streaming.” 32

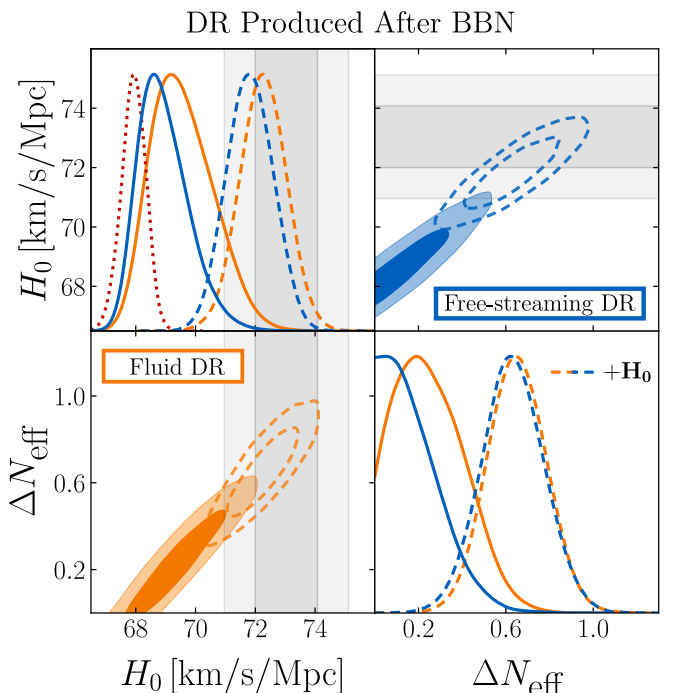


FIG. 3: 1- and 2-d posterior distributions for H_0 and ΔN_{eff} in models with dark radiation produced after BBN. We compare our results obtained with our baseline dataset (solid curves/shaded contours) with those obtained by combining with the determination of H_0 from SH₀ES (dashed curves/contours). The 1-d H_0 posterior for Λ CDM with the baseline dataset is shown by the dotted curve. 34

measurement is shown by the gray shaded bands (1– and 2 σ) in Fig. 1. Within the context of fluid DR, as can be also appreciated in Fig. 1. We report two measures of tension in Table I: one based on a simple Gaussian estimate (GT) which is commonly employed in the literature but leads to overestimates when the posteriors are asymmetric, as in our case; the second measure partially corrects for this by using the true posterior distribution from our MCMC analysis (IT), as suggested in [57] and reviewed in Appendix A. We estimate the tension to be around 2.5σ within the fluid model, and around 3σ in the free-streaming scenario, when we do not include constraints from primordial elements (the tension is further lowered by $\sim 0.3\sigma$ using P18+DESI alone, see App. B 1). These results represent a significant alleviation of the H_0 tension within these models. Comparing to results obtained with previous BAO data, we find that DESI reduces the tension by $(0.5 – 1)\sigma$ depending on the model, see Fig. 2. The $\Delta\chi^2$ for all models and datasets considered here with respect to Λ CDM is close to zero. 31

IV. The Hubble tension 33

Our findings (especially for the fluid DR model) open the possibility to interpret the Hubble tension as a mild to moderate statistical fluctuation within the context of the Λ CDM + ΔN_{eff} models presented above. 37 Additional constraints from primordial elements from [51, 52] worsen the tension in all models. However, 38

Parameter	P20_H+DESI		P18+DESI 107	
	+Pantheon_Plus	+DES-SN5YR	+Pantheon_Plus	+DES-SN5YR 70
ΔN_{eff}	0.35 (0.18) _{-0.20} ^{0.15} ₃₅	0.31 (0.31) _{-0.21} ^{0.13} ₃₅	0.26 (0.34) _{-0.21} ^{0.11} ₃₅	0.231 (0.019) _{-0.22} ^{0.062} ₄₅₂₀
$H_0 [\text{km/s/Mpc}]$	70.0 (69.4) _{-1.3} ^{1.3} ₃₅	69.54 (69.78) _{-1.2} ^{0.92} ₃₅	69.56 (69.82) _{-1.2} ^{0.83} ₁₉₀	69.13 (68.07) _{-1.2} ^{0.79} ₇₀
$H_0 \text{ GT}$	2.05σ	2.52σ	2.59σ	2.99σ ₃₅
$H_0 \text{ IT}$	1.87σ	2.21σ	2.28σ	2.51σ ₃₅
$\Delta\chi^2$	-0.2	-0.6	-0.4	-0.2 ₃₅
ΔAIC	1.8	1.4	1.6	1.8 ₃₅

TABLE III: Marginalized posteriors for ΔN_{eff} and H_0 for fluid dark radiation produced after BBN with different datasets. 36

they are avoided if the dark radiation is produced after the epoch of BBN and sufficiently before recombination. This specification does not introduce any additional parameters, nor does it lead to a coincidence problem (in contrast to models where a fluid is taken to undergo a transition around the epoch of recombination, such as [58–62]), since DR can still be produced in a redshift range that spans around five orders of magnitude, corresponding to $eV \lesssim T \lesssim 100 \text{ keV}$. 38

Beside the relevance of primordial element constraints, a difference arises if DR is indeed produced after BBN, compared to the previous case which implicitly assumed production before BBN. In the latter case, DR alters the theoretical prediction of Y_{He} , which then affects the number density of electrons at recombination $n_e(z) \propto (1 - Y_{\text{He}})$ (see e.g. [63] for a recent discussion). Therefore, when considering the scenario where DR is produced after BBN, we determine Y_{He} by setting $\Delta N_{\text{eff}} = 0$ at BBN. We compare the inferences made with our baseline dataset for both fluid and free-streaming DR produced after BBN in Table II. Interestingly, we find an additional reduction of the H_0 tension (and relaxation of constraints on ΔN_{eff}), and a $\gtrsim 1\sigma$ preference for fluid DR persists. 39

Having estimated the tension in DR models with production after BBN to be around $(2.3 - 2.8)\sigma$ compared to the ΛCDM model, we combine our baseline dataset with the SH₀ES determination of H_0 . Results are presented in the rightmost columns of Table II and in Fig. 3. Remarkably, we find evidence at the 5 σ (4.5σ) level for fluid (free-streaming) DR, and a negligible residual tension with SH₀ES. This is accompanied by a very significant improvement in χ^2 with respect to the ΛCDM model. We account for the additional parameter via the Akaike Information Criterion (AIC) [64] (see also [65]) $\Delta\text{AIC} \equiv \Delta\chi^2 + 2 \times (\# \text{ of added free parameters})$ and report $\Delta\text{AIC} \simeq -23(-19)$ for fluid (free-streaming) DR. 40

Our results are robust when fitting to more recent CMB and supernovae likelihoods/data. We present in Fig. 4 and Table III results for the fluid DR model using the Planck PR4 Hillpop/Lollipop likelihoods (P20_H [66]) and the DES-SN5YR supernovae dataset [67]. With P20_H, which has displayed a resolution to the anomalous amplitude of the lensing power spectrum A_L in previous Planck likelihoods [68], we find even

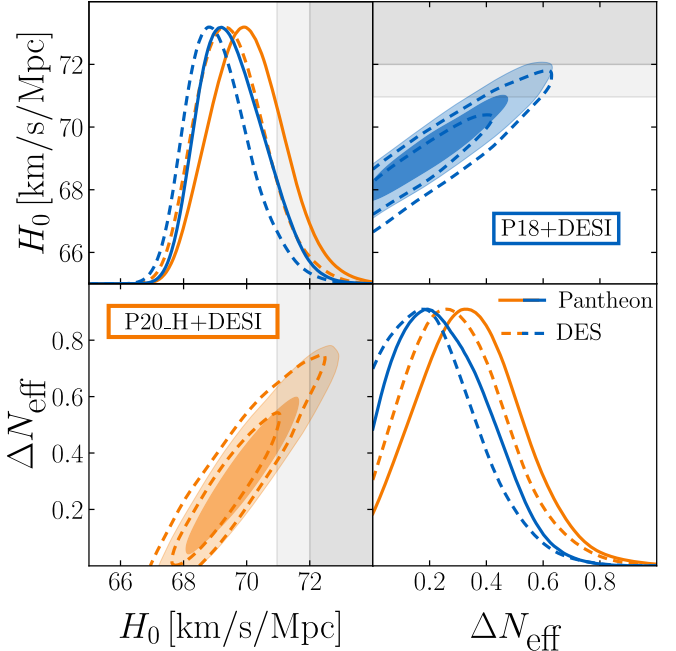


FIG. 4: 1- and 2-d posterior distributions for H_0 and ΔN_{eff} for fluid DR produced after BBN with different datasets. 41

further evidence for ΔN_{eff} and a reduced H_0 tension to $\sim 1.9\sigma$ (when combining with +Pantheon_Plus). With DES-SN5YR, we see an overall consistent picture with our baseline dataset. In addition, when comparing to the recently released value of H_0 from SH₀ES [69], the tensions we have presented worsen by at most 0.3σ . 42

In all the models and combination of datasets used in this work, we find posteriors for the matter clustering parameter $S_8 \equiv \sigma_8 \sqrt{\Omega_m}/0.3$ in agreement with the most recent measurements from weak lensing surveys [70]. 43

Finally, we have focused here on perhaps the simplest DR scenarios, but it is conceivable that analogous conclusions could apply to other scenarios that lead to a similar evolution for the cosmological background, for instance models with varying Newton constant, see e.g. [71]. 44

V. Discussion 45

The large improvements in the goodness-of-the-fit which we find are of course driven by the SH₀ES measurement, and have been reported to a similar level in the past for other models with previous BAO data. Therefore, one may doubt the relevance of our results. However, we would like to stress two crucial differences with such previous findings. First, our results are obtained by combining datasets that are in $\sim 2.5\sigma$ tension with each other within the context of DR models when production occurs only after BBN, especially for the fluid DR case (removing Pantheon+ data further reduces the tension to even $\sim 2\sigma$, see Appendix B 1). Second, the models under consideration are simple, one-parameter extensions of Λ CDM, with several possible implementations in particle physics. 46

Perhaps the simplest example of DR production after BBN, which can arise in a broad class of models, is a massive particle, the abundance of which is negligible in the pre-BBN era, and that decays to some light states after BBN (see e.g. [72–78]), with a decay rate $10^{-37} \text{ GeV} \lesssim \Gamma \lesssim 10^{-27} \text{ GeV}$. Other possibilities exist in the literature for the production of DR after BBN; see, for instance, [79–81]. 47

Our work provides new state-of-the-art bounds on dark radiation models, that partially relax constraints on beyond the SM physics and should prove important for model building. 48

Remarkably, our findings also suggest that the new BAO data open the possibility to address the Hubble tension with well-motivated minimal extensions of Λ CDM model. 49

With a conservative perspective, the possibility that our findings are driven by a statistical fluctuation or underestimated systematic uncertainties in the DESI measurement (which exhibit some discrepancy with previous BAO data) should be kept in mind, and will be decisively clarified soon by upcoming data releases from DESI itself and Euclid, see e.g. [82], where the 1σ error on ΔN_{eff} for the free streaming case from Euclid power spectrum and lensing measurements is forecasted to be 0.05. 50

Acknowledgments

We thank Héctor Gil-Marín for help with DESI data, and María Vincenzi and Dillon Brout for help with the DES-SN5YR likelihood. The work of F.R. is supported by the grant RYC2021-031105-I from the Ministerio de Ciencia e Innovación (Spain). I.J.A. is supported by NASA grant 80NSSC22K081. The work of A.N. is supported by the grants PID2019-108122GB-C32 from the Spanish Ministry of Science and Innovation, Unit of Excellence María de Maeztu 2020-2023 of ICCUB (CEX2019-000918-M) and AGAUR 2021 SGR 00872. A.N. is grateful to the Physics Department of the University of Florence for the hospitality during the course of this work. We acknowledge use of the Tufts HPC research cluster and the INFN Florence cluster. 51

-
- [1] S. Bashinsky and U. Seljak, Neutrino perturbations in CMB anisotropy and matter clustering, *Phys. Rev. D* **69**, 083002 (2004), arXiv:astro-ph/0310198. 97
 - [2] Z. Hou, R. Keisler, L. Knox, M. Millea, and C. Reichardt, How Massless Neutrinos Affect the Cosmic Microwave Background Damping Tail, *Phys. Rev. D* **87**, 083008 (2013), arXiv:1104.2333 [astro-ph.CO]. 98
 - [3] D. Baumann, D. Green, J. Meyers, and B. Wallisch, Phases of New Physics in the CMB, *JCAP* **01**, 007, arXiv:1508.06342 [astro-ph.CO]. 99
 - [4] S. Aiola *et al.* (ACT), The Atacama Cosmology Telescope: DR4 Maps and Cosmological Parameters, *JCAP* **12**, 047, arXiv:2007.07288 [astro-ph.CO]. 100
 - [5] J. A. Sobrin *et al.* (SPT-3G), The Design and Integrated Performance of SPT-3G, *Astrophys. J. Supp.* **258**, 42 (2022), arXiv:2106.11202 [astro-ph.IM]. 100
 - [6] L. Amendola *et al.*, Cosmology and fundamental physics with the Euclid satellite, *Living Rev. Rel.* **21**, 2 (2018), arXiv:1606.00180 [astro-ph.CO]. 102
 - [7] v. Ivezić *et al.* (LSST), LSST: from Science Drivers to Reference Design and Anticipated Data Products, *Astrophys. J.* **873**, 111 (2019), arXiv:0805.2366 [astro-ph]. 103
 - [8] K. Abazajian *et al.* (CMB-S4), Snowmass 2021 CMB-S4 White Paper, (2022), arXiv:2203.08024 [astro-ph.CO]. 130
 - [9] P. Ade *et al.* (Simons Observatory), The Simons Observatory: Science goals and forecasts, *JCAP* **02**, 056, arXiv:1808.07445 [astro-ph.CO]. 105
 - [10] A. G. Adame *et al.* (DESI), DESI 2024 III: Baryon Acoustic Oscillations from Galaxies and Quasars, (2024), arXiv:2404.03000 [astro-ph.CO]. 106
 - [11] A. G. Adame *et al.* (DESI), DESI 2024 IV: Baryon Acoustic Oscillations from the Lyman Alpha Forest, (2024), arXiv:2404.03001 [astro-ph.CO]. 106
 - [12] A. G. Adame *et al.* (DESI), DESI 2024 VI: Cosmological Constraints from the Measurements of Baryon Acoustic Oscillations, (2024), arXiv:2404.03002 [astro-ph.CO]. 106
 - [13] F. Beutler, C. Blake, M. Colless, D. H. Jones, L. Staveley-Smith, L. Campbell, Q. Parker, W. Saunders, and F. Watson, The 6dF Galaxy Survey: Baryon Acoustic Oscillations and the Local Hubble Constant, *Mon. Not. Roy. Astron. Soc.* **416**, 3017 (2011), arXiv:1106.3366 [astro-ph.CO]. 109
 - [14] A. J. Ross, L. Samushia, C. Howlett, W. J. Percival, A. Burden, and M. Manera, The clustering of the SDSS DR7 main Galaxy sample – I. A 4 per cent distance measure at $z = 0.15$, *Mon. Not. Roy. Astron. Soc.* **449**, 835 (2015), arXiv:1409.3242 [astro-ph.CO]. 110
 - [15] S. Satpathy *et al.* (BOSS), The clustering of galaxies in the completed SDSS-III Baryon Oscillation Spectroscopic Survey: On the measurement of growth rate using galaxy correlation functions, *Mon. Not. Roy. Astron. Soc.* **469**, 111

- 1369 (2017), arXiv:1607.03148 [astro-ph.CO]. 130
- [16] N. Aghanim *et al.* (Planck), Planck 2018 results. VI. Cosmological parameters, *Astron. Astrophys.* **641**, A6 (2020), [Erratum: *Astron. Astrophys.* 652, C4 (2021)], arXiv:1807.06209 [astro-ph.CO]. 112
- [17] N. Aghanim *et al.* (Planck), Planck 2018 results. V. CMB power spectra and likelihoods, *Astron. Astrophys.* **641**, A5 (2020), arXiv:1907.12875 [astro-ph.CO]. 112
- [18] T.-H. Yeh, J. Shelton, K. A. Olive, and B. D. Fields, Probing physics beyond the standard model: limits from BBN and the CMB independently and combined, *JCAP* **10**, 046, arXiv:2207.13133 [astro-ph.CO]. 114
- [19] M. S. Turner, Thermal Production of Not SO Invisible Axions in the Early Universe, *Phys. Rev. Lett.* **59**, 2489 (1987), [Erratum: *Phys. Rev. Lett.* 60, 1101 (1988)]. 115
- [20] E. W. Kolb and M. S. Turner, *The Early Universe*, Vol. 69 (1990). 57
- [21] Z. G. Berezhiani, A. S. Sakharov, and M. Y. Khlopov, Primordial background of cosmological axions, *Sov. J. Nucl. Phys.* **55**, 1063 (1992). 57
- [22] S. Chang and K. Choi, Hadronic axion window and the big bang nucleosynthesis, *Phys. Lett. B* **316**, 51 (1993), arXiv:hep-ph/9306216. 118
- [23] E. Masso, F. Rota, and G. Zsembinszki, On axion thermalization in the early universe, *Phys. Rev. D* **66**, 023004 (2002), arXiv:hep-ph/0203221. 119
- [24] R. Z. Ferreira, A. Notari, and F. Rompineve, Dine-Fischler-Srednicki-Zhitnitsky axion in the CMB, *Phys. Rev. D* **103**, 063524 (2021), arXiv:2012.06566 [hep-ph]. 120
- [25] A. Notari, F. Rompineve, and G. Villadoro, Improved Hot Dark Matter Bound on the QCD Axion, *Phys. Rev. Lett.* **131**, 011004 (2023), arXiv:2211.03799 [hep-ph]. 122
- [26] F. D'Eramo, R. Z. Ferreira, A. Notari, and J. L. Bernal, Hot Axions and the H_0 tension, *JCAP* **11**, 014, arXiv:1808.07430 [hep-ph]. 122
- [27] R. Z. Ferreira and A. Notari, Observable Windows for the QCD Axion Through the Number of Relativistic Species, *Phys. Rev. Lett.* **120**, 191301 (2018), arXiv:1801.06090 [hep-ph]. 123
- [28] D. Baumann, D. Green, and B. Wallisch, New Target for Cosmic Axion Searches, *Phys. Rev. Lett.* **117**, 171301 (2016), arXiv:1604.08614 [astro-ph.CO]. 123
- [29] Z. Chacko, Y. Cui, S. Hong, and T. Okui, Hidden dark matter sector, dark radiation, and the CMB, *Phys. Rev. D* **92**, 055033 (2015), arXiv:1505.04192 [hep-ph]. 121
- [30] M. A. Buen-Abad, G. Marques-Tavares, and M. Schmaltz, Non-Abelian dark matter and dark radiation, *Phys. Rev. D* **92**, 023531 (2015), arXiv:1505.03542 [hep-ph]. 126
- [31] Z. Chacko, Y. Cui, S. Hong, T. Okui, and Y. Tsai, Partially Acoustic Dark Matter, Interacting Dark Radiation, and Large Scale Structure, *JHEP* **12**, 108, arXiv:1609.03569 [astro-ph.CO]. 127
- [32] S. Nakagawa, F. Takahashi, and W. Yin, Early dark energy by a dark Higgs field and axion-induced nonthermal trapping, *Phys. Rev. D* **107**, 063016 (2023), arXiv:2209.01107 [astro-ph.CO]. 128
- [33] F.-Y. Cyr-Racine, K. Sigurdson, J. Zavala, T. Bringmann, M. Vogelsberger, and C. Pfrommer, ETHOS—an effective theory of structure formation: From dark particle physics to the matter distribution of the Universe, *Phys. Rev. D* **93**, 123527 (2016), arXiv:1512.05344 [astro-ph.CO]. 129
- [34] J. Lesgourgues, G. Marques-Tavares, and M. Schmaltz, Evidence for dark matter interactions in cosmological precision data?, *JCAP* **02**, 037, arXiv:1507.04351 [astro-ph.CO]. 113
- [35] C. Brust, Y. Cui, and K. Sigurdson, Cosmological Constraints on Interacting Light Particles, *JCAP* **08**, 020, arXiv:1703.10732 [astro-ph.CO]. 112
- [36] M. A. Buen-Abad, M. Schmaltz, J. Lesgourgues, and T. Bringmann, Interacting Dark Sector and Precision Cosmology, *JCAP* **01**, 008, arXiv:1708.09406 [astro-ph.CO]. 114
- [37] M. Archidiacono, D. C. Hooper, R. Murgia, S. Bohr, J. Lesgourgues, and M. Viel, Constraining Dark Matter Dark Radiation interactions with CMB, BAO, and Lyman- α , *JCAP* **10**, 055, arXiv:1907.01496 [astro-ph.CO]. 115
- [38] N. Blinov and G. Marques-Tavares, Interacting radiation after Planck and its implications for the Hubble Tension, *JCAP* **09**, 029, arXiv:2003.08387 [astro-ph.CO]. 115
- [39] D. Scolnic *et al.*, The Pantheon+ Analysis: The Full Data Set and Light-curve Release, *Astrophys. J.* **938**, 113 (2022), arXiv:2112.03863 [astro-ph.CO]. 135
- [40] A. G. Riess *et al.*, A Comprehensive Measurement of the Local Value of the Hubble Constant with 1 km s $^{-1}$ Mpc $^{-1}$ Uncertainty from the Hubble Space Telescope and the SH0ES Team, *Astrophys. J. Lett.* **934**, L7 (2022), arXiv:2112.04510 [astro-ph.CO]. 136
- [41] K. C. Wong *et al.*, H0LiCOW – XIII. A 2.4 per cent measurement of H_0 from lensed quasars: 5.3 σ tension between early- and late-Universe probes, *Mon. Not. Roy. Astron. Soc.* **498**, 1420 (2020), arXiv:1907.04869 [astro-ph.CO]. 137
- [42] D. Scolnic, A. G. Riess, J. Wu, S. Li, G. S. Anand, R. Beaton, S. Casertano, R. I. Anderson, S. Dhawan, and X. Ke, CATS: The Hubble Constant from Standardized TRGB and Type Ia Supernova Measurements, *Astrophys. J. Lett.* **954**, L31 (2023), arXiv:2304.06693 [astro-ph.CO]. 138
- [43] W. L. Freedman, Measurements of the Hubble Constant: Tensions in Perspective, *Astrophys. J.* **919**, 16 (2021), arXiv:2106.15656 [astro-ph.CO]. 139
- [44] C.-P. Ma and E. Bertschinger, Cosmological perturbation theory in the synchronous and conformal Newtonian gauges, *Astrophys. J.* **455**, 7 (1995), arXiv:astro-ph/9506072. 140
- [45] J. Lesgourgues, The Cosmic Linear Anisotropy Solving System (CLASS) I: Overview, (2011), arXiv:1104.2932 [astro-ph.IM]. 141
- [46] D. Blas, J. Lesgourgues, and T. Tram, The Cosmic Linear Anisotropy Solving System (CLASS) II: Approximation schemes, *JCAP* **07**, 034, arXiv:1104.2933 [astro-ph.CO]. 142
- [47] B. Audren, J. Lesgourgues, K. Benabed, and S. Prunet, Conservative Constraints on Early Cosmology: an illustration of the Monte Python cosmological parameter inference code, *JCAP* **02**, 001, arXiv:1210.7183 [astro-ph.CO]. 143
- [48] T. Brinckmann and J. Lesgourgues, MontePython 3: boosted MCMC sampler and other features, *Phys. Dark Univ.* **24**, 100260 (2019), arXiv:1804.07261 [astro-ph.CO]. 144
- [49] A. Lewis, GetDist: a Python package for analysing Monte Carlo samples, (2019), arXiv:1910.13970 [astro-ph.IM]. 145
- [50] S. Alam *et al.* (BOSS), The clustering of galaxies in the completed SDSS-III Baryon Oscillation Spectroscopic Survey: cosmological analysis of the DR12 galaxy

- sample, *Mon. Not. Roy. Astron. Soc.* **470**, 2617 (2017), arXiv:1607.03155 [astro-ph.CO]. 146
- [51] E. Aver, K. A. Olive, and E. D. Skillman, The effects of He I λ 10830 on helium abundance determinations, *JCAP* **07**, 011, arXiv:1503.08146 [astro-ph.CO]. 147
- [52] R. J. Cooke, M. Pettini, and C. C. Steidel, One Percent Determination of the Primordial Deuterium Abundance, *Astrophys. J.* **855**, 102 (2018), arXiv:1710.11129 [astro-ph.CO]. 148
- [53] L. E. Marcucci, G. Mangano, A. Kievsky, and M. Viviani, Implication of the proton-deuteron radiative capture for Big Bang Nucleosynthesis, *Phys. Rev. Lett.* **116**, 102501 (2016), [Erratum: Phys. Rev. Lett. 117, 049901 (2016)], arXiv:1510.07877 [nucl-th]. 149
- [54] E. Aver, D. A. Berg, K. A. Olive, R. W. Pogge, J. J. Salzer, and E. D. Skillman, Improving helium abundance determinations with Leo P as a case study, *JCAP* **03**, 027, arXiv:2010.04180 [astro-ph.CO]. 150
- [55] Y. I. Izotov, T. X. Thuan, and N. G. Guseva, A new determination of the primordial He abundance using the He I λ 10830 Å emission line: cosmological implications, *Mon. Not. Roy. Astron. Soc.* **445**, 778 (2014), arXiv:1408.6953 [astro-ph.CO]. 151
- [56] N. Schöneberg, J. Lesgourgues, and D. C. Hooper, The BAO+BBN take on the Hubble tension, *JCAP* **10**, 029, arXiv:1907.11594 [astro-ph.CO]. 152
- [57] M. Raveri and C. Doux, Non-Gaussian estimates of tensions in cosmological parameters, *Phys. Rev. D* **104**, 043504 (2021), arXiv:2105.03324 [astro-ph.CO]. 153
- [58] V. Poulin, T. L. Smith, T. Karwal, and M. Kamionkowski, Early Dark Energy Can Resolve The Hubble Tension, *Phys. Rev. Lett.* **122**, 221301 (2019), arXiv:1811.04083 [astro-ph.CO]. 154
- [59] F. Niedermann and M. S. Sloth, New early dark energy, *Phys. Rev. D* **103**, L041303 (2021), arXiv:1910.10739 [astro-ph.CO]. 155
- [60] M. Gonzalez, M. P. Hertzberg, and F. Rompineve, Ultralight Scalar Decay and the Hubble Tension, *JCAP* **10**, 028, arXiv:2006.13959 [astro-ph.CO]. 156
- [61] I. J. Allali, M. P. Hertzberg, and F. Rompineve, Dark sector to restore cosmological concordance, *Phys. Rev. D* **104**, L081303 (2021), arXiv:2104.12798 [astro-ph.CO]. 157
- [62] D. Aloni, A. Berlin, M. Joseph, M. Schmaltz, and N. Weiner, A Step in understanding the Hubble tension, *Phys. Rev. D* **105**, 123516 (2022), arXiv:2111.00014 [astro-ph.CO]. 158
- [63] F.-Y. Cyr-Racine, F. Ge, and L. Knox, Symmetry of Cosmological Observables, a Mirror World Dark Sector, and the Hubble Constant, *Phys. Rev. Lett.* **128**, 201301 (2022), arXiv:2107.13000 [astro-ph.CO]. 159
- [64] H. Akaike, A new look at the statistical model identification, *IEEE Transactions on Automatic Control* **19**, 716 (1974). 160
- [65] A. R. Liddle, Information criteria for astrophysical model selection, *Mon. Not. Roy. Astron. Soc.* **377**, L74 (2007), arXiv:astro-ph/0701113. 161
- [66] M. Tristram *et al.*, Cosmological parameters derived from the final Planck data release (PR4), *Astron. Astrophys.* **682**, A37 (2024), arXiv:2309.10034 [astro-ph.CO]. 162
- [67] T. M. C. Abbott *et al.* (DES), The Dark Energy Survey: Cosmology Results With ~1500 New High-redshift Type Ia Supernovae Using The Full 5-year Dataset, (2024), arXiv:2401.02929 [astro-ph.CO]. 163
- [68] G. E. Addison, C. L. Bennett, M. Halpern, G. Hinshaw, and J. L. Weiland, Revisiting the A_L Lensing Anomaly in Planck 2018 Temperature Data, (2023), arXiv:2310.03127 [astro-ph.CO]. 164
- [69] L. Breuval, A. G. Riess, S. Casertano, W. Yuan, L. M. Macri, M. Romaniello, Y. S. Murakami, D. Scolnic, G. S. Anand, and I. Soszyński, Small Magellanic Cloud Cepheids Observed with the Hubble Space Telescope Provide a New Anchor for the SH0ES Distance Ladder, (2024), arXiv:2404.08038 [astro-ph.CO]. 165
- [70] T. M. C. Abbott *et al.* (Kilo-Degree Survey, Dark Energy Survey), DES Y3 + KiDS-1000: Consistent cosmology combining cosmic shear surveys, *Open J. Astrophys.* **6**, 2305.17173 (2023), arXiv:2305.17173 [astro-ph.CO]. 166
- [71] G. Ballesteros, A. Notari, and F. Rompineve, The H_0 tension: ΔG_N vs. ΔN_{eff} , *JCAP* **11**, 024, arXiv:2004.05049 [astro-ph.CO]. 167
- [72] K. Ichikawa, M. Kawasaki, K. Nakayama, M. Senami, and F. Takahashi, Increasing effective number of neutrinos by decaying particles, *JCAP* **05**, 008, arXiv:hep-ph/0703034. 168
- [73] W. Fischler and J. Meyers, Dark Radiation Emerging After Big Bang Nucleosynthesis?, *Phys. Rev. D* **83**, 063520 (2011), arXiv:1011.3501 [astro-ph.CO]. 169
- [74] D. Hooper, F. S. Queiroz, and N. Y. Gnedin, Non-Thermal Dark Matter Mimicking An Additional Neutrino Species In The Early Universe, *Phys. Rev. D* **85**, 063513 (2012), arXiv:1111.6599 [astro-ph.CO]. 170
- [75] O. E. Bjaelde, S. Das, and A. Moss, Origin of Delta N_{eff} as a Result of an Interaction between Dark Radiation and Dark Matter, *JCAP* **10**, 017, arXiv:1205.0553 [astro-ph.CO]. 171
- [76] K. Choi, K.-Y. Choi, and C. S. Shin, Dark radiation and small-scale structure problems with decaying particles, *Phys. Rev. D* **86**, 083529 (2012), arXiv:1208.2496 [hep-ph]. 172
- [77] J. Hasenkamp and J. Kersten, Dark radiation from particle decay: cosmological constraints and opportunities, *JCAP* **08**, 024, arXiv:1212.4160 [hep-ph]. 173
- [78] A. C. Sobotka, A. L. Erickcek, and T. L. Smith, Comprehensive constraints on dark radiation injection after BBN, *Phys. Rev. D* **109**, 063538 (2024), arXiv:2312.13235 [astro-ph.CO]. 173
- [79] R. Z. Ferreira, A. Notari, O. Pujolas, and F. Rompineve, Gravitational waves from domain walls in Pulsar Timing Array datasets, *JCAP* **02**, 001, arXiv:2204.04228 [astro-ph.CO]. 175
- [80] D. Aloni, M. Joseph, M. Schmaltz, and N. Weiner, Dark Radiation from Neutrino Mixing after Big Bang Nucleosynthesis, *Phys. Rev. Lett.* **131**, 221001 (2023), arXiv:2301.10792 [astro-ph.CO]. 176
- [81] M. Garny, F. Niedermann, H. Rubira, and M. S. Sloth, Hot New Early Dark Energy bridging cosmic gaps: Supercooled phase transition reconciles (stepped) dark radiation solutions to the Hubble tension with BBN, (2024), arXiv:2404.07256 [astro-ph.CO]. 177
- [82] T. Brinckmann, D. C. Hooper, M. Archidiacono, J. Lesgourgues, and T. Sprenger, The promising future of a robust cosmological neutrino mass measurement, *JCAP* **01**, 059, arXiv:1808.05955 [astro-ph.CO]. 178
- [83] I. J. Allali, F. Rompineve, and M. P. Hertzberg, Dark sectors with mass thresholds face cosmological datasets, *Phys. Rev. D* **108**, 023527 (2023), arXiv:2305.14166 [astro-ph.CO]. 179

Appendix

A. Tension Measures 53

For the assessment of tension between the H_0 measurement of the SH₀ES collaboration and the inferences made in this work, we define the following metrics. First, the commonly used measure of “Gaussian tension” (GT) is defined as 54

$$GT = \frac{|\mu_m - \mu_{MC}|}{\sqrt{\sigma_m^2 + \sigma_{MC}^2}} \quad (A1) \quad 24$$

□

where μ_m and μ_{MC} are the mean values of H_0 determined by the SH₀ES collaboration and by our MCMC analyses, respectively. σ_m^2 is the variance for the SH₀ES measurement. For the variance of the MCMC inference σ_{MC}^2 , we take the upper 1σ error derived from our marginalized posteriors on H_0 . Since the posteriors for H_0 we derive are not symmetric, there is not a clear choice of whether to average the upper and lower σ , or to take the value that is on the side of the distribution closest to the SH₀ES measurement (upper). In this work, we take σ_{MC} to always be the upper derived σ such that we do not underestimate the tension. 56

To address the non-gaussian nature of our inferred posteriors, we employ also the measure which we term the “integrated tension” (IT) [57, 83], defined via 57

$$\int_{-\infty}^{\infty} P_{MC}(h) \frac{1}{2} \left(1 \pm \text{erf} \left(\frac{h - \mu_m}{\sqrt{2}\sigma_m} \right) \right) dh = \int_{-\infty}^{\infty} \frac{1}{\sqrt{2\pi}} e^{-\frac{1}{2}x^2} dx \quad (A2) \quad 70$$

To understand this formula, let us examine each side. The left hand side is the integral over the cross-correlation of the two posterior distributions, namely the posterior distribution derived from our MCMC $P_{MC}(h)$, and the posterior from the SH₀ES measurement. In Eq. (A2), we have already integrated the SH₀ES posterior, assuming it to be purely gaussian, and therefore all that remains are the mean and standard deviation μ_m and σ_m . Using the posterior distribution from a given MCMC, the left hand side constitutes a probability (understood as the probability of measuring the SH₀ES value given the posterior from MCMC). Then, the right hand side of Eq. (A2) equates this probability with the integral over a gaussian (with mean= 0 and variance= 1), and one solves for the upper limit of the integral IT which gives this same probability. For example, if the left hand side of Eq. (A2) gives a probability of 68%, then we obtain the measure of tension to be $IT = 1\sigma$. 58

B. Detailed Posteriors 59

We present in the following sections the detailed posteriors we obtain when evaluating the several models discussed in this work against several combinations of datasets. Appendices B1 to B7 present tables and plots of posteriors for the models: Λ CDM, Free-streaming dark radiation, Fluid dark radiation, and Neutrinos. The title of each section gives the combination of data explored in that section. Then, Appendix B8 and Appendix B9 explore the posteriors with a variety of datasets on the models of dark radiation produced after BBN for fluid and free-streaming, respectively. 60

1. P18+DESI 70

Parameter	Λ CDM	Free-streaming DR	Fluid DR	Neutrinos
$100\omega_b$	2.249 (2.248) _{-0.013} ^{+0.013}	2.262 (2.264) _{-0.016} ^{+0.016}	2.272 (2.274) _{-0.019} ^{+0.017}	2.256 (2.25) _{-0.017} ^{+0.019}
ω_{cdm}	0.11811 (0.11823) _{-0.00086} ^{+0.00087}	0.1208 (0.1212) _{-0.0024} ^{+0.0019}	0.1224 (0.1205) _{-0.0031} ^{+0.0021}	0.1193 (0.1176) _{-0.0028} ^{+0.0024}
$\ln 10^{10} A_s$	3.054 (3.057) _{-0.016} ^{+0.014}	3.062 (3.055) _{-0.017} ^{+0.015}	3.052 (3.041) _{-0.016} ^{+0.015}	3.058 (3.057) _{-0.018} ^{+0.015}
n_s	0.9689 (0.9689) _{-0.0036} ^{+0.0036}	0.9748 (0.9742) _{-0.0057} ^{+0.0047}	0.9712 (0.9678) _{-0.0039} ^{+0.0039}	0.9713 (0.9715) _{-0.0065} ^{+0.0064}
τ_{reio}	0.0608 (0.0608) _{-0.0081} ^{+0.0081}	0.0614 (0.0595) _{-0.0083} ^{+0.0072}	0.0619 (0.053) _{-0.0084} ^{+0.0072}	0.0615 (0.0641) _{-0.0087} ^{+0.0067}
ΔN_{eff}		< 0.395	0.25 (0.13) _{-0.18} ^{+0.11}	0.12 (0.062) _{-0.16} ^{+0.10}
$\sum m_\nu$	< 0.119	< 0.124	< 0.127	< 0.116
H_0 [km/s/Mpc]	68.09 (68.18) _{-0.40} ^{+0.43}	69.10 (68.91) _{-0.95} ^{+0.66}	69.75 (69.19) _{-1.2} ^{+0.87}	68.5 (68.4) _{-0.99} ^{+1.1}
S_8	0.813 (0.818) _{-0.010} ^{+0.010}	0.814 (2.483) _{-0.011} ^{+0.011}	0.812 (0.809) _{-0.010} ^{+0.010}	0.816 (0.807) _{-0.010} ^{+0.011}
H_0 GT	4.4σ	3.2σ	2.43σ	3.0σ
H_0 IT	4.12σ	2.81σ	2.17σ	3.08σ

TABLE IV: Marginalized posteriors for various model parameters for the Λ CDM, Free-streaming DR, Fluid DR, and Neutrino models, fitting to the dataset: **P18+DESI**. All upper bounds are reported at 95% C.L., for any case where the 1σ lower bound is overlapping with our priors. 63

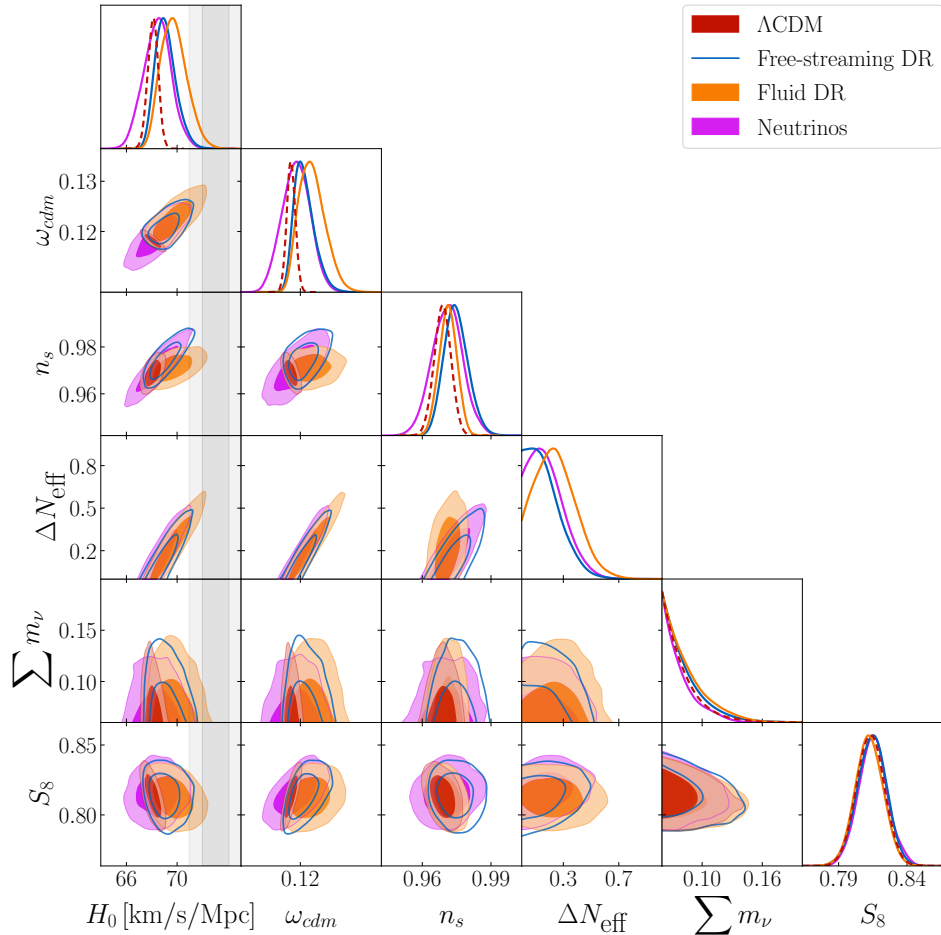


FIG. 5: One and two-dimensional posterior distributions for various model parameters for the Λ CDM, Free-streaming DR, Fluid DR, and Neutrino models, fitting to the dataset: **P18+DESI**. The 68% and 95% confidence intervals from the measurement of H_0 by SH0ES are shown in the gray and lighter gray shaded regions. 72

2. P18+DESI+Pantheon_Plus 62

Parameter	Λ CDM	Free-streaming DR	Fluid DR	Neutrinos 62
$100\omega_b$	$2.247 (2.251)^{+0.013}_{-0.013}$	$2.258 (2.246)^{+0.015}_{-0.016} 62$	$2.265 (2.257)^{+0.017}_{-0.019} 80$	$2.248 (2.256)^{+0.019}_{-0.018} 66$
ω_{cdm}	$0.11844 (0.11856)^{+0.00084}_{-0.00086}$	$0.1211 (0.1192)^{+0.0014}_{-0.0025} 60$	$0.1223 (0.1212)^{+0.0020}_{-0.0030} 80$	$0.1186 (0.1191)^{+0.0028}_{-0.0031} 62$
$\ln 10^{10} A_s$	$3.054 (3.061)^{+0.015}_{-0.016} 66$	$3.061 (3.039)^{+0.014}_{-0.017} 66$	$3.050 (3.055)^{+0.015}_{-0.015} 80$	$3.054 (3.052)^{+0.014}_{-0.018} 66$
n_s	$0.9681 (0.9679)^{+0.0039}_{-0.0036} 66$	$0.9734 (0.9689)^{+0.0043}_{-0.0058} 60$	$0.9699 (0.9667)^{+0.0037}_{-0.0039} 80$	$0.9685 (0.9759)^{+0.0068}_{-0.0069} 62$
τ_{reio}	$0.0602 (0.0636)^{+0.0074}_{-0.0083} 66$	$0.0606 (0.0537)^{+0.0071}_{-0.0082} 30$	$0.0605 (0.0619)^{+0.0072}_{-0.0080} 80$	$0.0601 (0.0608)^{+0.0071}_{-0.0086} 66$
ΔN_{eff}		< 0.386	$0.221 (0.128)^{+0.088}_{-0.18} 66$	$0.06 (0.143)^{+0.14}_{-0.19} 66$
$\sum m_\nu$	< 0.123	< 0.137	< 0.132	< 0.127
H_0 [km/s/Mpc]	$67.93 (68.07)^{+0.44}_{-0.38} 66$	$68.79 (67.99)^{+0.60}_{-0.89} 66$	$69.35 (68.72)^{+0.81}_{-1.1} 62$	$68.0 (67.14)^{+0.97}_{-1.2} 70$
S_8	$0.817 (0.822)^{+0.010}_{-0.010} 66$	$0.818 (0.436)^{+0.010}_{-0.011} 66$	$0.8161 (0.825)^{+0.0099}_{-0.0099} 62$	$0.817 (0.821)^{+0.011}_{-0.011} 74$
M_b	$-19.424 (-19.421)^{+0.013}_{-0.011} 66$	$19.396 (-19.426)^{+0.017}_{-0.028} 66$	$19.381 (-19.4)^{+0.024}_{-0.033} 66$	$19.422 (-19.448)^{+0.030}_{-0.036} 60$
H_0 GT	4.53σ	3.53σ	2.81σ	$3.54\sigma 66$
H_0 IT	3.93σ	3.06σ	2.52σ	$3.22\sigma 66$

TABLE V: Marginalized posteriors for various model parameters for the Λ CDM, Free-streaming DR, Fluid DR, and Neutrino models, fitting to the dataset: **P18+DESI+Pantheon_Plus**. All upper bounds are reported at 95% C.L., for any case where the 1σ lower bound is overlapping with our priors. 75

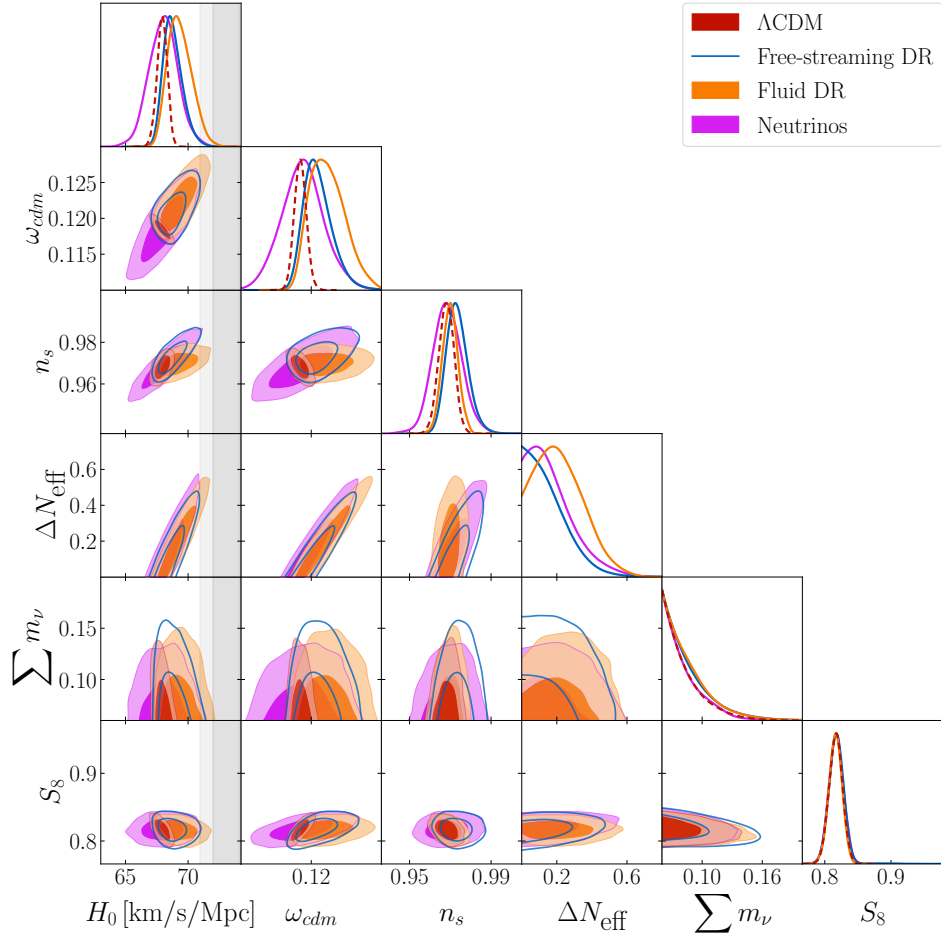


FIG. 6: One and two-dimensional posterior distributions for various model parameters for the Λ CDM, Free-streaming DR, Fluid DR, and Neutrino models, fitting to the dataset: **P18+DESI+Pantheon_Plus**. The 68% and 95% confidence intervals from the measurement of H_0 by SH0ES are shown in the gray and lighter gray shaded regions. 80

3. P18+DESI+Pantheon Plus+H₀ 70

Parameter	Λ CDM	Free-streaming DR	Fluid DR	Neutrinos 62
$100\omega_b$	$2.264 (2.275)^{+0.013}_{-0.013}$	$2.290 (2.289)^{+0.015}_{-0.015}$	$2.304 (2.307)^{+0.015}_{-0.015}$	$2.291 (2.285)^{+0.014}_{-0.014}$
ω_{cdm}	$0.11682 (0.11669)^{+0.00083}_{-0.00083}$	$0.1263 (0.126)^{+0.0025}_{-0.0025}$	$0.1281 (0.1286)^{+0.0019}_{-0.0016}$	$0.1263 (0.1268)^{+0.0024}_{-0.0024}$
$\ln 10^{10} A_s$	$3.061 (3.07)^{+0.015}_{-0.016}$	$3.078 (3.079)^{+0.015}_{-0.017}$	$3.048 (3.042)^{+0.015}_{-0.016}$	$3.078 (3.065)^{+0.016}_{-0.016}$
n_s	$0.9723 (0.9732)^{+0.0037}_{-0.0036}$	$0.9871 (0.9867)^{+0.0049}_{-0.0050}$	$0.9746 (0.972)^{+0.0036}_{-0.0039}$	$0.9872 (0.9873)^{+0.0049}_{-0.0050}$
τ_{reio}	$0.0651 (0.0666)^{+0.0074}_{-0.0085}$	$0.0634 (0.0636)^{+0.0072}_{-0.0086}$	$0.0633 (0.0588)^{+0.0074}_{-0.0077}$	$0.0633 (0.0567)^{+0.0073}_{-0.0084}$
ΔN_{eff}		$0.54 (0.52)^{+0.13}_{-0.13}$	$0.592 (0.611)^{+0.091}_{-0.060}$	$0.59 (0.619)^{+0.13}_{-0.13}$
$\sum m_\nu$	< 0.099	< 0.126	< 0.131	< 0.118
H_0 km/s/Mpc	$68.82 (68.98)^{+0.37}_{-0.39}$	$71.47 (71.39)^{+0.73}_{-0.76}$	$72.13 (72.25)^{+0.61}_{-0.41}$	$71.46 (71.79)^{+0.73}_{-0.73}$
S_8	$0.8017 (0.8045)^{+0.0096}_{-0.010}$	$0.822 (0.824)^{+0.011}_{-0.011}$	$0.8095 (0.8086)^{+0.0097}_{-0.010}$	$0.821 (0.819)^{+0.011}_{-0.011}$
M_b	$-19.398 (-19.392)^{+0.011}_{-0.011}$	$19.320 (-19.319)^{+0.021}_{-0.021}$	$19.301 (-19.295)^{+0.017}_{-0.011}$	$19.320 (-19.311)^{+0.021}_{-0.021}$
H_0 GT	3.82σ	1.23σ	0.75σ	1.24σ
H_0 IT	3.8σ	1.23σ	0.76σ	1.24σ
$\Delta\chi^2$	—	—19.1	—23.8	—17.5
ΔAIC	—	—17.1	—21.8	—15.5

TABLE VI: Marginalized posteriors for various model parameters for the Λ CDM, Free-streaming DR, Fluid DR, and Neutrino models, fitting to the dataset: **P18+DESI+Pantheon Plus+H₀**. All upper bounds are reported at 95% C.L., for any case where the 1σ lower bound is overlapping with our priors.

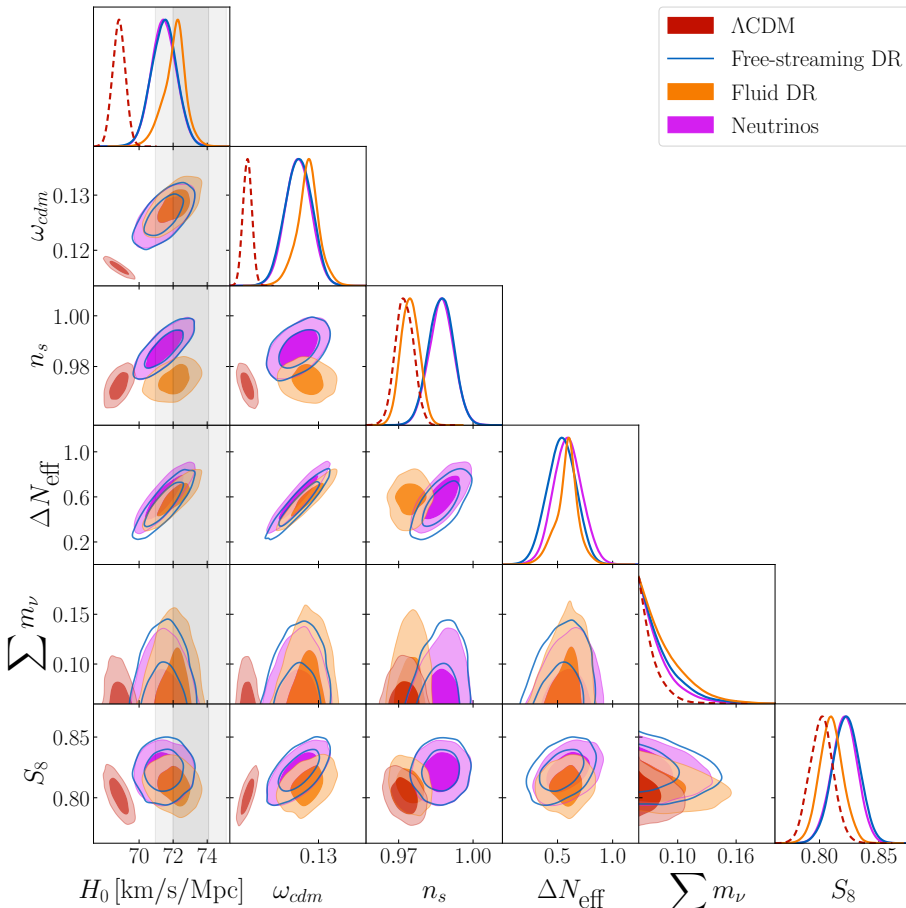


FIG. 7: One and two-dimensional posterior distributions for various model parameters for the Λ CDM, Free-streaming DR, Fluid DR, and Neutrino models, fitting to the dataset: **P18+DESI+Pantheon Plus+H₀**. The 68% and 95% confidence intervals from the measurement of H_0 by SH₀ES are shown in the gray and lighter gray shaded regions.

4. P18+DESI+Y_{He}, D/H 10

Parameter	Λ CDM	Free-streaming DR	Fluid DR	Neutrinos	62
$100\omega_b$	2.249 (2.24) $^{+0.013}_{-0.013}$	2.254 (2.25) $^{+0.015}_{-0.017}$ 62	2.266 (2.27) $^{+0.016}_{-0.018}$ 82	2.250 (2.23) $^{+0.017}_{-0.018}$ 73	
ω_{cdm}	0.11812 (0.11808) $^{+0.00089}_{-0.00087}$ 90	0.1212 (0.1206) $^{+0.0016}_{-0.0021}$ 94	0.1212 (0.1205) $^{+0.0018}_{-0.0026}$ 94	0.1183 (0.1166) $^{+0.0026}_{-0.0026}$ 74	
$\ln 10^{10} A_s$	3.055 (3.051) $^{+0.013}_{-0.015}$ 74	3.061 (3.06) $^{+0.013}_{-0.015}$ 74	3.053 (3.061) $^{+0.015}_{-0.016}$ 57	3.055 (3.058) $^{+0.016}_{-0.016}$ 70	
n_s	0.9689 (0.9676) $^{+0.0039}_{-0.0035}$ 74	0.9743 (0.9754) $^{+0.0050}_{-0.0057}$	0.9707 (0.9723) $^{+0.0039}_{-0.0039}$	0.9693 (0.9629) $^{+0.0064}_{-0.0062}$ 62	
τ_{reio}	0.0610 (0.0587) $^{+0.0071}_{-0.0082}$ 74	0.0605 (0.061) $^{+0.0072}_{-0.0083}$	0.0619 (0.0642) $^{+0.0074}_{-0.0083}$	0.0611 (0.0655) $^{+0.0071}_{-0.0083}$ 74	
ΔN_{eff}		0.179 (0.136) $^{+0.073}_{-0.15}$ 74	0.182 (0.148) $^{+0.061}_{-0.17}$ 86	0.06 (-0.078) $^{+0.16}_{-0.16}$ 74	
$\sum m_\nu$	< 0.121	< 0.125	< 0.127	< 0.118	74
H_0 [km/s/Mpc]	68.09 (68.17) $^{+0.42}_{-0.41}$ 74	69.00 (68.86) $^{+0.69}_{-0.93}$ 74	69.30 (69.39) $^{+0.71}_{-1.0}$ 141	68.2 (67.2) $^{+1.0}_{-1.0}$ 70	
S_8	0.814 (0.814) $^{+0.010}_{-0.010}$ 74	0.817 (1.829) $^{+0.010}_{-0.011}$ 74	0.813 (0.816) $^{+0.011}_{-0.010}$ 141	0.814 (0.822) $^{+0.011}_{-0.011}$ 74	
H_0 GT	4.42σ	3.23σ	2.97σ	3.37σ	74
H_0 IT	3.95σ	2.99σ	2.66σ	3.31σ	74

TABLE VII: Marginalized posteriors for various model parameters for the Λ CDM, Free-streaming DR, Fluid DR, and Neutrino models, fitting to the dataset: **P18+DESI+Y_{He}, D/H**. All upper bounds are reported at 95% C.L., for any case where the 1σ lower bound is overlapping with our priors. 79

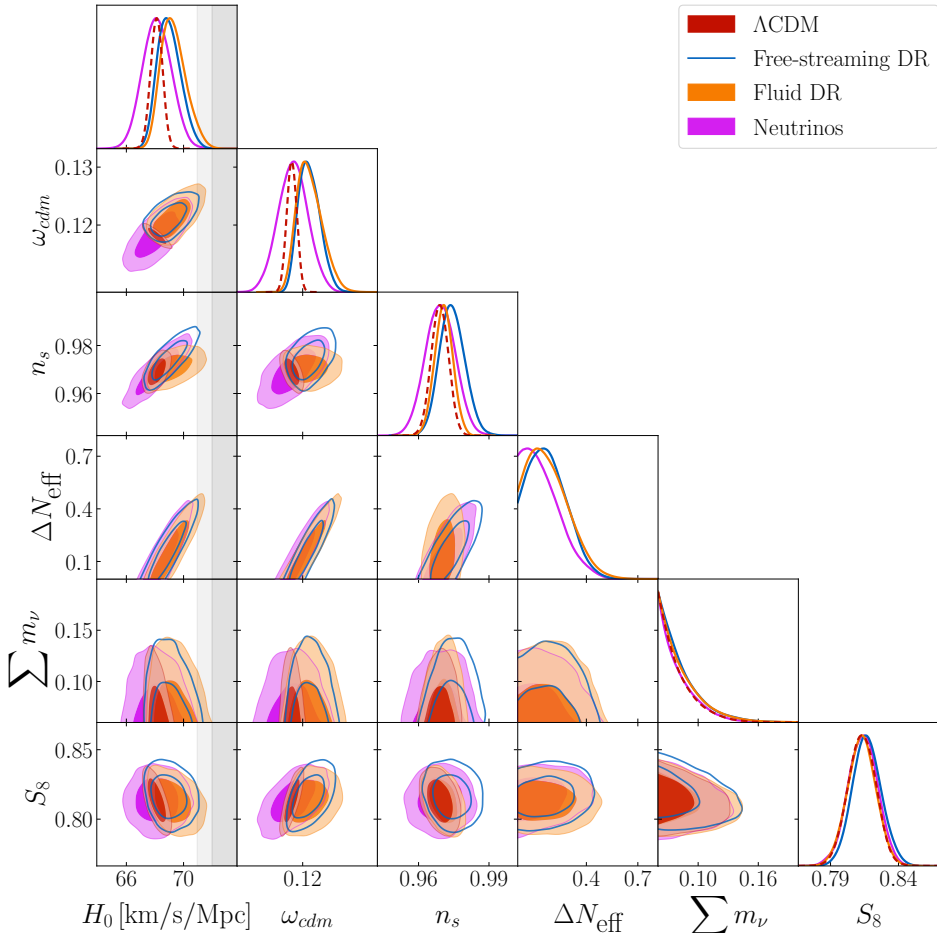


FIG. 8: One and two-dimensional posterior distributions for various model parameters for the Λ CDM, Free-streaming DR, Fluid DR, and Neutrino models, fitting to the dataset: **P18+DESI+Y_{He}, D/H**. The 68% and 95% confidence intervals from the measurement of H_0 by SH0ES are shown in the gray and lighter gray shaded regions. 88

5. P18+DESI+Y_{He}, D/H+Pantheon_Plus

Parameter	Λ CDM	Free-streaming DR	Fluid DR	Neutrinos 62
$100\omega_b$	$2.247 (2.251)^{+0.014}_{-0.014}$	$2.254 (2.255)^{+0.014}_{-0.014}$	$2.260 (2.242)^{+0.016}_{-0.016}$	$2.249 (2.238)^{+0.015}_{-0.015}$
ω_{cdm}	$0.11845 (0.11833)^{+0.00084}_{-0.00084}$	$0.1203 (0.1196)^{+0.0013}_{-0.0020}$	$0.1213 (0.1187)^{+0.0016}_{-0.0024}$	$0.1191 (0.1183)^{+0.0015}_{-0.0025}$
$\ln 10^{10} A_s$	$3.053 (3.055)^{+0.014}_{-0.014}$	$3.059 (3.061)^{+0.015}_{-0.017}$	$3.052 (3.045)^{+0.015}_{-0.015}$	$3.055 (3.034)^{+0.014}_{-0.014}$
n_s	$0.9680 (0.9677)^{+0.0035}_{-0.0038}$	$0.9721 (0.9728)^{+0.0043}_{-0.0049}$	$0.9694 (0.9694)^{+0.0037}_{-0.0037}$	$0.9695 (0.9662)^{+0.0050}_{-0.0065}$
τ_{reio}	$0.0602 (0.0606)^{+0.0069}_{-0.0081}$	$0.0607 (0.0625)^{+0.0071}_{-0.0084}$	$0.0608 (0.058)^{+0.0071}_{-0.0082}$	$0.0599 (0.0519)^{+0.0082}_{-0.0084}$
ΔN_{eff}		< 0.295	< 0.365	$0.087 (-0.007)^{+0.076}_{-0.15}$
$\sum m_\nu$	< 0.121	< 0.125	< 0.131	< 0.130
H_0 [km/s/Mpc]	$67.92 (68.09)^{+0.41}_{-0.41}$	$68.58 (68.89)^{+0.55}_{-0.69}$	$68.97 (68.0)^{+0.65}_{-0.93}$	$68.13 (67.53)^{+0.68}_{-0.96}$
S_8	$0.817 (0.817)^{+0.010}_{-0.0098}$	$0.819 (0.816)^{+0.010}_{-0.011}$	$0.816 (0.819)^{+0.010}_{-0.010}$	$0.817 (0.818)^{+0.010}_{-0.0097}$
M_b	$-19.424 (-19.421)^{+0.012}_{-0.012}$	$19.404 (-19.393)^{+0.010}_{-0.021}$	$19.392 (-19.423)^{+0.020}_{-0.028}$	$19.418 (-19.436)^{+0.020}_{-0.029}$
H_0 GT	4.58σ	3.8σ	3.31σ	3.96σ
H_0 IT	3.79σ	3.42σ	2.93σ	3.68σ

TABLE VIII: Marginalized posteriors for various model parameters for the Λ CDM, Free-streaming DR, Fluid DR, and Neutrino models, fitting to the dataset: **P18+DESI+Y_{He}, D/H+Pantheon_Plus**. All upper bounds are reported at 95% C.L., for any case where the 1σ lower bound is overlapping with our priors. 83

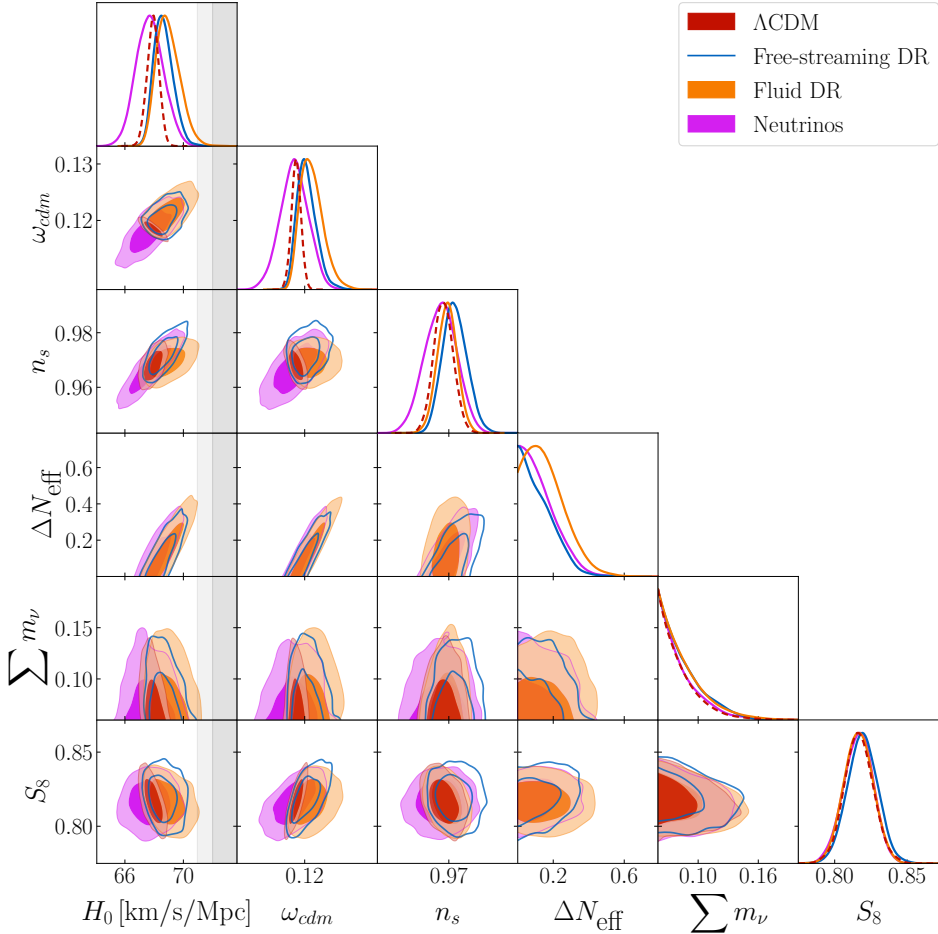


FIG. 9: One and two-dimensional posterior distributions for various model parameters for the Λ CDM, Free-streaming DR, Fluid DR, and Neutrino models, fitting to the dataset: **P18+DESI+Y_{He}, D/H+Pantheon_Plus**. The 68% and 95% confidence intervals from the measurement of H_0 by SH0ES are shown in the gray and lighter gray shaded regions.

6. P18+DESI+Y_{He}, D/H+Pantheon_Plus+H₀

Parameter	ΛCDM	Free-streaming DR	Fluid DR	Neutrinos [62]
$100\omega_b$	$2.264 (2.273)^{+0.013}_{-0.013}$	$2.285 (2.28)^{+0.014}_{-0.014}$	$2.295 (2.296)^{+0.015}_{-0.015}$	$2.287 (2.284)^{+0.015}_{-0.014}$
ω_{cdm}	$0.11685 (0.11643)^{+0.00081}_{-0.00081}$	$0.1248 (0.1238)^{+0.0019}_{-0.0019}$	$0.1260 (0.1256)^{+0.0024}_{-0.0024}$	$0.1244 (0.1229)^{+0.0023}_{-0.0023}$
$\ln 10^{10} A_s$	$3.060 (3.068)^{+0.015}_{-0.017}$	$3.076 (3.057)^{+0.013}_{-0.017}$	$3.051 (3.042)^{+0.015}_{-0.017}$	$3.075 (3.063)^{+0.016}_{-0.017}$
n_s	$0.9723 (0.9721)^{+0.0053}_{-0.0036}$	$0.9849 (0.9825)^{+0.0048}_{-0.0047}$	$0.9742 (0.9747)^{+0.0037}_{-0.0037}$	$0.9844 (0.9832)^{+0.0050}_{-0.0049}$
τ_{reio}	$0.0647 (0.0677)^{+0.0073}_{-0.0084}$	$0.0635 (0.0557)^{+0.0071}_{-0.0087}$	$0.0636 (0.0604)^{+0.0070}_{-0.0087}$	$0.0639 (0.0615)^{+0.0074}_{-0.0084}$
ΔN_{eff}		$0.45 (0.38)^{+0.10}_{-0.10}$	$0.48 (0.48)^{+0.11}_{-0.11}$	$0.49 (0.431)^{+0.12}_{-0.12}$
$\sum m_\nu$	< 0.099	< 0.120	< 0.128	< 0.115
$H_0 [\text{km/s/Mpc}]$	$68.81 (69.12)^{+0.37}_{-0.37}$	$71.02 (70.59)^{+0.69}_{-0.67}$	$71.46 (71.78)^{+0.74}_{-0.73}$	$70.95 (71.06)^{+0.70}_{-0.70}$
S_8	$0.8015 (0.8005)^{+0.0098}_{-0.0098}$	$0.817 (2.701)^{+0.010}_{-0.010}$	$0.8090 (0.8007)^{+0.0099}_{-0.010}$	$0.817 (0.807)^{+0.011}_{-0.011}$
M_b	$-19.398 (-19.387)^{+0.011}_{-0.011}$	$19.332 (-19.341)^{+0.019}_{-0.020}$	$19.321 (-19.31)^{+0.021}_{-0.021}$	$19.335 (-19.332)^{+0.020}_{-0.020}$
H_0 GT	3.83σ	1.62σ	1.24σ	1.67σ
H_0 IT	3.84σ	1.62σ	1.24σ	1.67σ
$\Delta\chi^2$	—	—12.7	—17.7	—10.5
ΔAIC	—	—10.7	—15.7	—8.5

TABLE IX: Marginalized posteriors for various model parameters for the ΛCDM , Free-streaming DR, Fluid DR, and Neutrino models, fitting to the dataset: **P18+DESI+Y_{He}, D/H+Pantheon_Plus+H₀**. All upper bounds are reported at 95% C.L., for any case where the 1 σ lower bound is overlapping with our priors. [91]

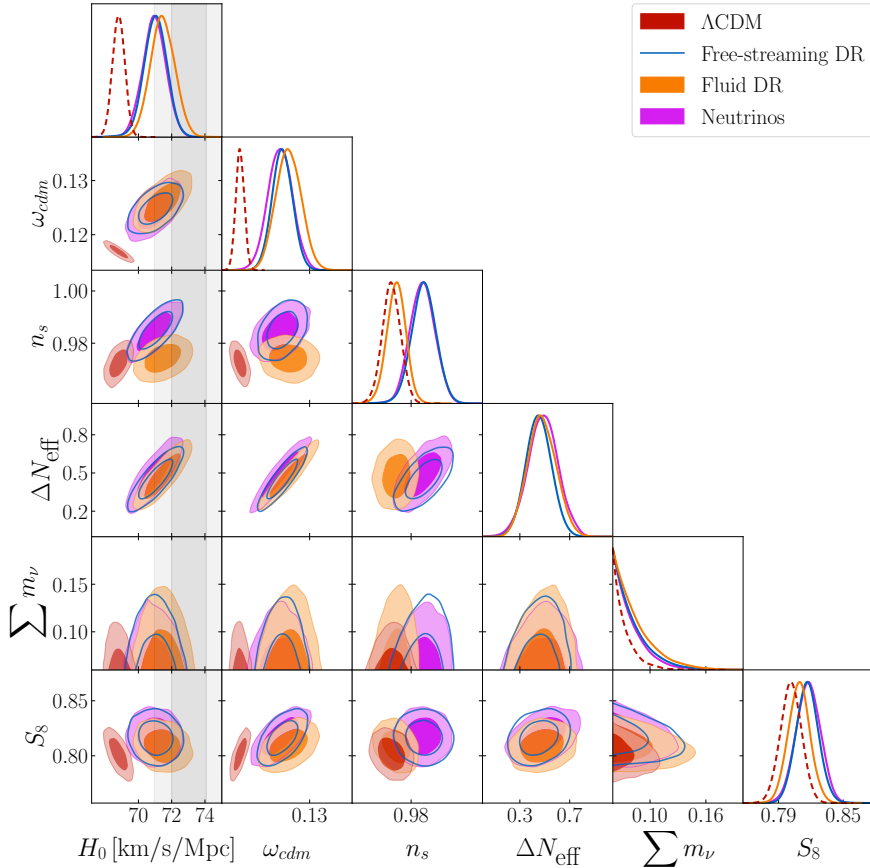


FIG. 10: One and two-dimensional posterior distributions for various model parameters for the ΛCDM , Free-streaming DR, Fluid DR, and Neutrino models, fitting to the dataset: **P18+DESI+Y_{He}, D/H+Pantheon_Plus+H₀**. The 68% and 95% confidence intervals from the measurement of H_0 by SH₀ES are shown in the gray and lighter gray shaded regions.

7. P18+SDSS+6dFGS+Pantheon_Plus 70

Parameter	Λ CDM	Free-streaming DR	Fluid DR	Neutrinos
$100\omega_b$	$2.238 (2.253)^{+0.013}_{-0.013}$	$2.246 (2.248)^{+0.015}_{-0.015}$	$2.251 (2.252)^{+0.016}_{-0.018}$	$2.232 (2.23)^{+0.018}_{-0.018}$
ω_{cdm}	$0.11964 (0.11931)^{+0.00090}_{-0.00089}$	$0.1217 (0.1202)^{+0.0012}_{-0.0023}$	$0.1223 (0.1204)^{+0.0013}_{-0.0025}$	$0.1183 (0.1177)^{+0.0028}_{-0.0031}$
$\ln 10^{10} A_s$	$3.049 (3.053)^{+0.013}_{-0.015}$	$3.055 (3.049)^{+0.014}_{-0.016}$	$3.048 (3.048)^{+0.015}_{-0.016}$	$3.045 (3.051)^{+0.016}_{-0.016}$
n_s	$0.9652 (0.9653)^{+0.0030}_{-0.0034}$	$0.9691 (0.9698)^{+0.0039}_{-0.0053}$	$0.9666 (0.9656)^{+0.0038}_{-0.0038}$	$0.9621 (0.9615)^{+0.0068}_{-0.0068}$
τ_{reio}	$0.0572 (0.0578)^{+0.0075}_{-0.0075}$	$0.0570 (0.0563)^{+0.0075}_{-0.0075}$	$0.0577 (0.056)^{+0.0068}_{-0.0080}$	$0.0568 (0.0597)^{+0.0067}_{-0.0075}$
ΔN_{eff}		< 0.312	< 0.285	$0.04 (-0.061)^{+0.18}_{-0.18}$
$\sum m_\nu$	< 0.152	< 0.174	< 0.169	< 0.146
H_0 [km/s/Mpc]	$67.27 (67.78)^{+0.43}_{-0.43}$	$67.84 (67.79)^{+0.58}_{-0.71}$	$68.25 (67.83)^{+0.69}_{-0.98}$	$66.8 (66.9)^{+1.1}_{-1.0}$
S_8	$0.827 (0.826)^{+0.011}_{-0.011}$	$0.826 (5.249)^{+0.012}_{-0.012}$	$0.826 (0.828)^{+0.011}_{-0.011}$	$0.826 (0.826)^{+0.011}_{-0.011}$
M_b	$-19.443 (-19.43)^{+0.013}_{-0.013}$	$19.421 (-19.426)^{+0.018}_{-0.026}$	$19.412 (-19.427)^{+0.021}_{-0.030}$	$19.458 (-19.455)^{+0.034}_{-0.035}$
H_0 GT	5.12σ	4.37σ	3.83σ	4.19σ
H_0 IT	5.11σ	3.53σ	3.35σ	4.24σ

TABLE X: Marginalized posteriors for various model parameters for the Λ CDM, Free-streaming DR, Fluid DR, and Neutrino models, fitting to the dataset: **P18+SDSS+6dFGS+Pantheon_Plus**. All upper bounds are reported at 95% C.L., for any case where the 1σ lower bound is overlapping with our priors. 95

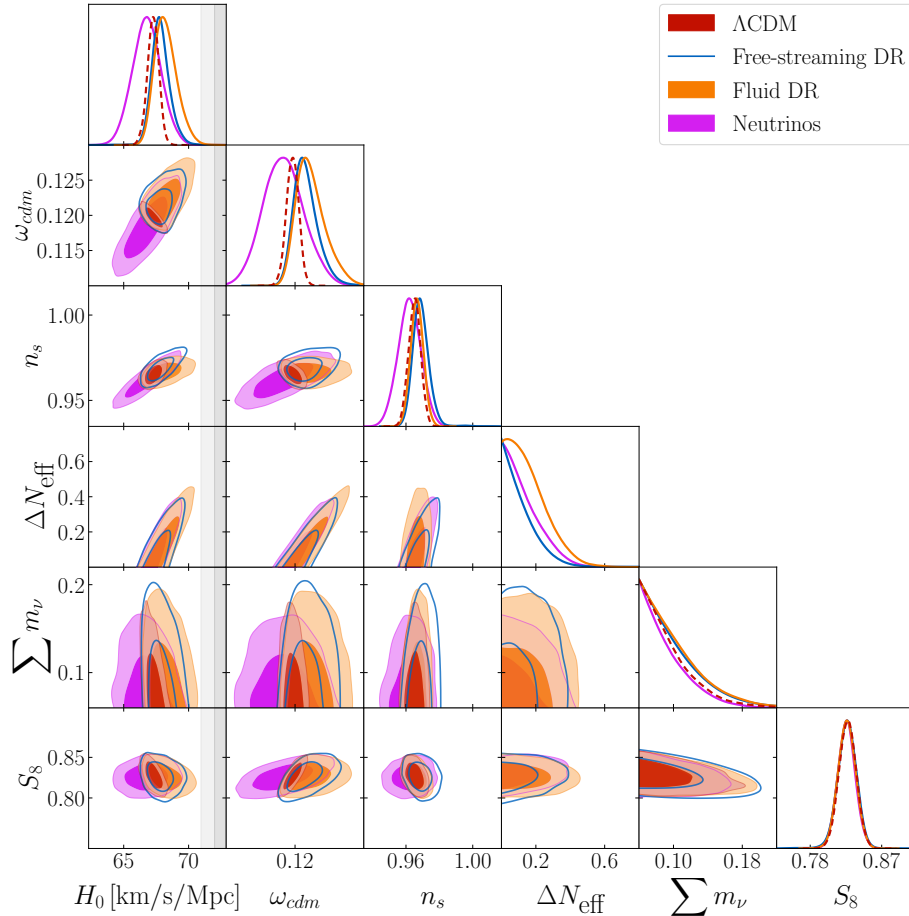


FIG. 11: One and two-dimensional posterior distributions for various model parameters for the Λ CDM, Free-streaming DR, Fluid DR, and Neutrino models, fitting to the dataset: **P18+SDSS+6dFGS+Pantheon_Plus**. The 68% and 95% confidence intervals from the measurement of H_0 by SH₀ES are shown in the gray and lighter gray shaded regions. 95

8. Fluid Dark Radiation Produced After BBN 89

Parameter	P18+SDSS+6dFGS+Pantheon_Plus	P18+DESI+Pantheon_Plus	P18+DESI+Pantheon_Plus+H ₀
100 ω_b	2.251 (2.241) _{-0.017} ^{+0.015}	2.266 (2.263) _{-0.014} ^{+0.015} ₉₀	2.299 (2.305) _{-0.015} ^{+0.015} ₇₈ ⁹⁰
ω_{cdm}	0.1228 (0.1219) _{-0.0028} ^{+0.0018} ₈₆	0.1229 (0.1254) _{-0.0034} ^{+0.0023} ₉₀	0.1291 (0.1303) _{-0.0028} ^{+0.0028} ₉₀
ln 10 ¹⁰ A _s	3.047 (3.049) _{-0.015} ^{+0.019} ₇₈	3.049 (3.041) _{-0.014} ^{+0.019} ₉₀	3.045 (3.053) _{-0.016} ^{+0.019} ₇₈
n _s	0.9658 (0.9652) _{-0.0037} ^{+0.0038} ₇₈	0.9689 (0.9666) _{-0.0037} ^{+0.0037} ₉₀	0.9716 (0.9759) _{-0.0035} ^{+0.0035} ₉₀
τ_{reio}	0.0575 (0.057) _{-0.0075} ^{+0.0069} ₈₂	0.0607 (0.057) _{-0.0081} ^{+0.0071} ₉₀	0.0627 (0.0679) _{-0.0083} ^{+0.0073} ₉₀
ΔN_{eff}	< 0.433	0.26 (0.34) _{-0.21} ^{+0.11} ₈₂	0.65 (0.73) _{-0.14} ^{+0.13} ₈₂
$\sum m_{\nu}$	< 0.166	< 0.137	< 0.149
H ₀ [km/s/Mpc]	68.39 (67.94) _{-1.1} ^{+0.71} ₈₆	69.56 (69.82) _{-1.2} ^{+0.85} ₉₀	72.25 (73.0) _{-0.73} ^{+0.79} ₉₆
S ₈	0.826 (0.834) _{-0.011} ^{+0.011} ₉₀	0.815 (0.825) _{-0.011} ^{+0.010} ₉₀	0.809 (0.812) _{-0.011} ^{+0.011} ₉₀
M _b	-19.408 (-19.42) _{-0.033} ^{+0.024} ₉₀	-19.374 (-19.365) _{-0.037} ^{+0.026} ₉₀	-19.298 (-19.276) _{-0.021} ^{+0.024} ₉₀
H ₀ GT	3.69 σ	2.59 σ	0.6 σ ₉₀
H ₀ IT	3.02 σ	2.28 σ	0.6 σ ₉₀
$\Delta\chi^2$	~ 0	-0.4	-24.7 ₉₀
ΔAIC	+2.0	+1.6	-22.7 ₂₉

TABLE XI: Marginalized posteriors for various model parameters for the Fluid DR model where the DR is produced after BBN. The fit is shown for the datasets P18+SDSS+6dFGS+Pantheon_Plus, P18+DESI+Pantheon_Plus, and P18+DESI+Pantheon_Plus+H₀. All upper bounds are reported at 95% C.L., for any case where the 1 σ lower bound is overlapping with our priors. 76
96 96

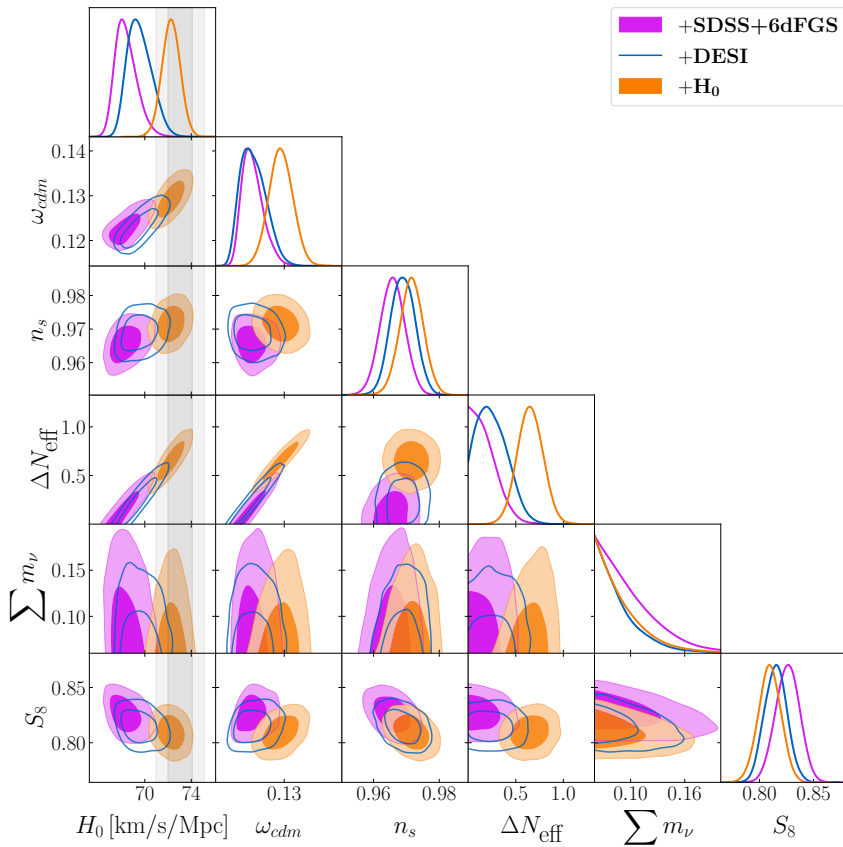


FIG. 12: One and two-dimensional posterior distributions for various model parameters for the Fluid DR model where the DR is produced after BBN. The fit is shown for the datasets P18+SDSS+6dFGS+Pantheon_Plus, P18+DESI+Pantheon_Plus, and P18+DESI+Pantheon_Plus+H₀. The 68% and 95% confidence intervals from the measurement of H₀ by SH₀ES are shown in the gray and lighter gray shaded regions. 64 64 64

9. Free-streaming Dark Radiation Produced After BBN 93

Parameter	P18+SDSS+6dFGS+Pantheon_Plus	P18+DESI+Pantheon_Plus	P18+DESI+Pantheon_Plus+H ₀
100 ω_b	2.245 (2.24) $^{+0.015}_{-0.014}$	2.257 (2.254) $^{+0.015}_{-0.014}$ 1.82	2.288 (2.278) $^{+0.014}_{-0.014}$ 1.70
ω_{cdm}	0.1219 (0.1218) $^{+0.0014}_{-0.0024}$ 94	0.1214 (0.1193) $^{+0.0016}_{-0.0027}$ 90	0.1278 (0.1287) $^{+0.0026}_{-0.0026}$ 94
ln 10 ¹⁰ A_s	3.054 (3.041) $^{+0.015}_{-0.016}$ 94	3.060 (3.059) $^{+0.014}_{-0.014}$ 94	3.077 (3.071) $^{+0.014}_{-0.014}$ 90
n_s	0.9688 (0.9676) $^{+0.0043}_{-0.0050}$ 94	0.9731 (0.9732) $^{+0.0045}_{-0.0055}$ 94	0.9864 (0.987) $^{+0.0044}_{-0.0047}$ 94
T_{reio}	0.0568 (0.0493) $^{+0.0068}_{-0.0073}$ 94	0.0602 (0.0623) $^{+0.0071}_{-0.0081}$ 94	0.0622 (0.0584) $^{+0.0069}_{-0.0084}$ 82
ΔN_{eff}	< 0.353	< 0.435	0.63 (0.65) $^{+0.14}_{-0.14}$ 94
$\sum m_\nu$	< 0.161	< 0.129	< 0.137
H_0 [km/s/Mpc]	68.03 (68.17) $^{+0.57}_{-0.57}$ 94	68.94 (68.41) $^{+0.63}_{-0.99}$ 94	71.82 (71.65) $^{+0.78}_{-0.77}$ 94
S_8	0.830 (0.826) $^{+0.011}_{-0.011}$ 94	0.821 (0.822) $^{+0.011}_{-0.011}$ 94	0.823 (0.83) $^{+0.011}_{-0.011}$ 94
M_b	-19.419 (-19.414) $^{+0.017}_{-0.026}$ 94	-19.393 (-19.41) $^{+0.019}_{-0.030}$ 94	-19.310 (-19.311) $^{+0.022}_{-0.022}$ 94
H_0 GT	4.22σ	3.37σ	0.94σ 94
H_0 IT	3.62σ	2.84σ	0.94σ 94
$\Delta\chi^2$	~ 0	+0.4	-20.5 94
ΔAIC	+2.0	+2.4	-18.5 94

TABLE XII: Marginalized posteriors for various model parameters for the Fluid DR model where the DR is produced after BBN. The fit is shown for the datasets P18+DESI+Pantheon_Plus and P18+DESI+Pantheon_Plus+H₀. All upper bounds are reported at 95% C.L., for any case where the 1 σ lower bound is overlapping with our priors.

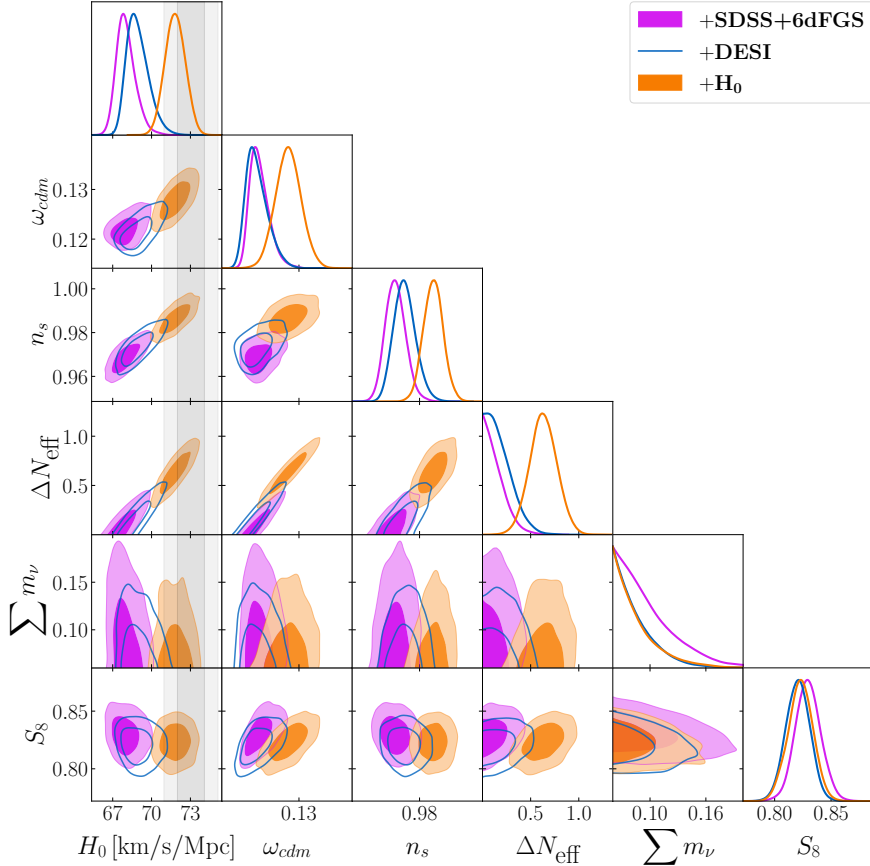


FIG. 13: One and two-dimensional posterior distributions for various model parameters for the free-streaming DR model where the DR is produced after BBN. The fit is shown for the datasets P18+DESI+Pantheon_Plus and P18+DESI+Pantheon_Plus+H₀. The 68% and 95% confidence intervals from the measurement of H_0 by SH0ES are shown in the gray and lighter gray shaded regions. 68 68 68